Vibration mitigation in offshore wind turbines via tuned mass damper

VIBRATION MITIGATION IN OFFSHORE WIND TURBINES VIA TUNED MASS DAMPER

Mina Ghassempour, Giuseppe Failla, Felice Arena

Department of Civil, Energy, Environmental and Materials Engineering (DICEAM)

University of Reggio Calabria, Via Graziella, Località Feo di Vito, 89122 Reggio Calabria

ABSTRACT

This paper deals with vibration mitigation via tuned mass damper in bottom-fixed, horizontal-axis offshore wind turbines. Focusing on a baseline 5-MW turbine mounted on a monopile, equipped with an omnidirectional tuned mass damper inside the nacelle, the study explores a wide range of potential tuning frequencies and mass ratios, in both operational and parked rotor conditions. It is found that the tuning frequency to attain optimal reduction of structural vibrations shall be changed depending on the wind velocity in operational conditions while, in contrast, is generally equal to the natural frequency of the first support-structure modes only in parked conditions. This result, attributable to inherent non-linearity of rotor dynamics, demonstrates that a conventional design of the tuned mass damper based on the natural frequencies of the support structure modes may not be suitable for offshore wind turbines.

KEYWORDS: Offshore wind turbine, Vibration mitigation, Tuned mass damper.

1. INTRODUCTION

As offshore wind farms gain increasing importance for power supply worldwide [1], vibration mitigation in offshore horizontal-axis wind turbines (HAWTs) has become a crucial issue to increase fatigue life and improve serviceability of the system under combined wind-wave loadings [2]. Recently,

several studies have addressed this problem, investigating the effectiveness of passive, semi-active as well as active devices, for bottom-fixed and floating supports.

For their simplicity, passive dampers have attracted a considerable attention and, in this context, especially tuned mass damper (TMD) devices have been studied [3]. Firstly, Lackner and Rotea [4] investigated the dynamic response of the baseline 5-MW HAWT developed by the National Renewable Energy Laboratory (NREL), mounted on an offshore monopile or a floating barge. They considered a TMD inside the nacelle acting in fore-aft direction, tuned to the natural frequency of the corresponding first support-structure mode. Upon developing an updated version of the aero-hydro-servo-elastic FAST code [5], named FAST-SC [4], the TMD damping providing optimal reduction of the tower top displacement standard deviation was identified via a free-vibration analysis and, then, fully-coupled simulations were implemented under simultaneous wind and wave loadings. For a given wind-wave state, several response indexes were calculated, including displacements/rotations as well as damage equivalent loads, and appreciable TMD performances were found for the barge but not for the monopile. This result was attributed to the fact that the main frequency content of the monopile response in fore-aft direction mirrors the frequency content of the wave loading, which is well below the natural frequency of the first fore-aft support-structure mode, i.e. the TMD tuning frequency [4]. Further investigations on the 5-MW NREL HAWT mounted on a monopile and three different floating supports (barge, spar-buoy and tension-leg platform), with a TMD placed inside the nacelle, were carried out by Stewart and Lackner [6]. In this case, they considered two independent TMDs, one in fore-aft direction and one in side-to-side direction, and developed proper simplified models of the support structure coupled with the TMD, in order to estimate the optimal TMD stiffness/mass/damping parameters providing best reduction of the tower top displacement standard deviation. Using a genetic algorithm different potential optimal sets were identified that, in general, corresponded to a TMD tuning frequency close to the natural frequency of the first fore-aft support structure mode. For two different wind-wave states, fully-coupled simulations in FAST-SC [4]-[5] showed that the TMD may be beneficial in terms of fatigue and ultimate load reductions, especially for barge and monopile. Specifically, reductions for the monopile were found more

in the side-to-side response than in the fore-aft response and, in agreement with ref. [4], this result was motivated observing that the side-to-side response is dominated by the first side-to-side support-structure mode while, instead, the frequency content of the fore-aft response mirrors the frequency content of the wind-wave loading, which is well below the natural frequency of the first fore-aft support-structure mode [6]. Effects of wind-wave misalignment and 45°-rotated configurations of the two TMDs were addressed by Stewart and Lackner in a further study [7], concluding that the primary impact of TMDs tuned to the natural frequencies of the first fore-aft and side-to-side support-structure modes is on the side-to-side response and, also, that the TMDs orientation does not affect significantly the loads. Still focusing on the 5-MW NREL HAWT on a monopile, Zuo et al. [8] proposed using multiple tuned mass dampers acting in fore-aft direction along the tower, in order to reduce vibrations under simultaneous wind, wave and earthquake excitations. The authors implemented a finite-element model of the structure in ABAQUS [9], with the rotor in a parked state. Upon a preliminary estimation of the TMDs parameters by an optimization procedure targeting the tower top displacement standard deviation, the relevant conclusions of the study were that multiple TMDs effectively mitigate vibrations involving the fundamental as well as the higher modes, as is typically the case under various excitation sources. Further, the effectiveness of a TMD acting in fore-aft direction inside floating supports was studied by Si et al., who focused on the OC3-Hywind spar [10].

Applications of passive TMDs were proposed also for land-based HAWTs and, specifically, by Altay et al. [11] for vibration control under wind and earthquake excitations, by Murtagh et al. under wind only [12]. In ref. [11] simulations were carried out in FAST-SC [4], while a simplified model of the structure as a uniform cantilever beam, with a top lumped mass modeling the nacelle and three cantilevers for parked blades, was adopted in ref. [12] using wind forces calculated from proper rotationally sampled wind spectra [13]. Again for land-based HAWTs, Enevoldsen and Mørk [14] studied the effects of a TMD using a linearized structural model acted upon by both rotationally and non-rotationally sampled wind spectra. In ref. [10]-[12]-[14], the TMD acted in fore-aft direction at the tower top and was tuned to the natural frequency of the first fore-aft support-structure mode.

With the purpose of vibration mitigation in offshore HAWTs, passive dampers alternative to the TMD concept have been also proposed. Examples are tuned liquid column damper (TLCD) devices placed in the nacelle, which proved effective in reducing tower-base bending moments [15] as well as improving structural reliability [16]. Active TMDs in the nacelle have been proposed for vibration mitigation of a floating barge [17]-[18]. Further, the application of dampers inside the rotor blades has been proposed by B. Fitzgerald et al [19], Arrigan et al. [20] and Zhang [21], considering active or passive TMDs, semi-active TMDs or roller dampers.

Building on the pioneering studies on TMD applications to offshore HAWTs [4]-[5]-[7]-[8], this paper focuses on the dynamic response of the 5-MW NREL HAWT mounted on an offshore monopile, equipped with an omnidirectional TMD inside the nacelle. Aero-hydro-servo-elastic simulations under simultaneous wind and wave loads are implemented in GH-BLADED [22]. The study starts from a preliminary dynamic analysis of the structure without TMD, which highlights inherent non-linearity of the response, and explores the TMD performances over a wide range of tuning frequencies, mass ratios, for several wind states, including operational and parked conditions. It will be demonstrated that, in order to achieve an optimal reduction in the standard deviation of the tower top displacement, the TMD may be tuned to the natural frequency of the first support-structure modes only in parked conditions while, instead, the tuning frequency shall be changed depending on the wind velocity in operational conditions. Insight in terms of TMD displacements and power production will also be given to assess feasibility of the TMD design at the optimal tuning frequencies.

The paper is organized as follows. The test structure is presented in Section 2. Simulation of wind-wave loads and TMD design are described in Sections 3 and 4. On discussing the system dynamics without TMD in Section 5, the system dynamics with TMD is investigated in Section 6.

2. TEST STRUCTURE

The test structure is taken from ref. [23]. The turbine is the baseline 5-MW NREL HAWT [24], a conventional three-bladed, upwind, variable-speed and variable blade-pitch-to-feather-controlled turbine,

which represents the reference conceptual model for several recent studies on land-based and offshore wind turbines [4]-[5]-[7]-[8]-[25]-[26]. The turbine is mounted on a steel tubular tower with steel monopile foundation, in a 20 m water depth. The geometry is described in Figure 1, steel parameters are: Young's modulus = 210 GPa, Shear modulus = 80.8 GPa, Mass density = 8500 kg/m^3 (density is higher than standard steel to account for additional mass of bolted/welded connections). Rotor blades are made of glass-fiber composite material, elastic properties at various stations along the blade are provided in the reference dataset [24]. In agreement with previous studies, it is assumed that the nacelle dimensions are 18×6×6 m, see ref. [4]-[5]-[7].

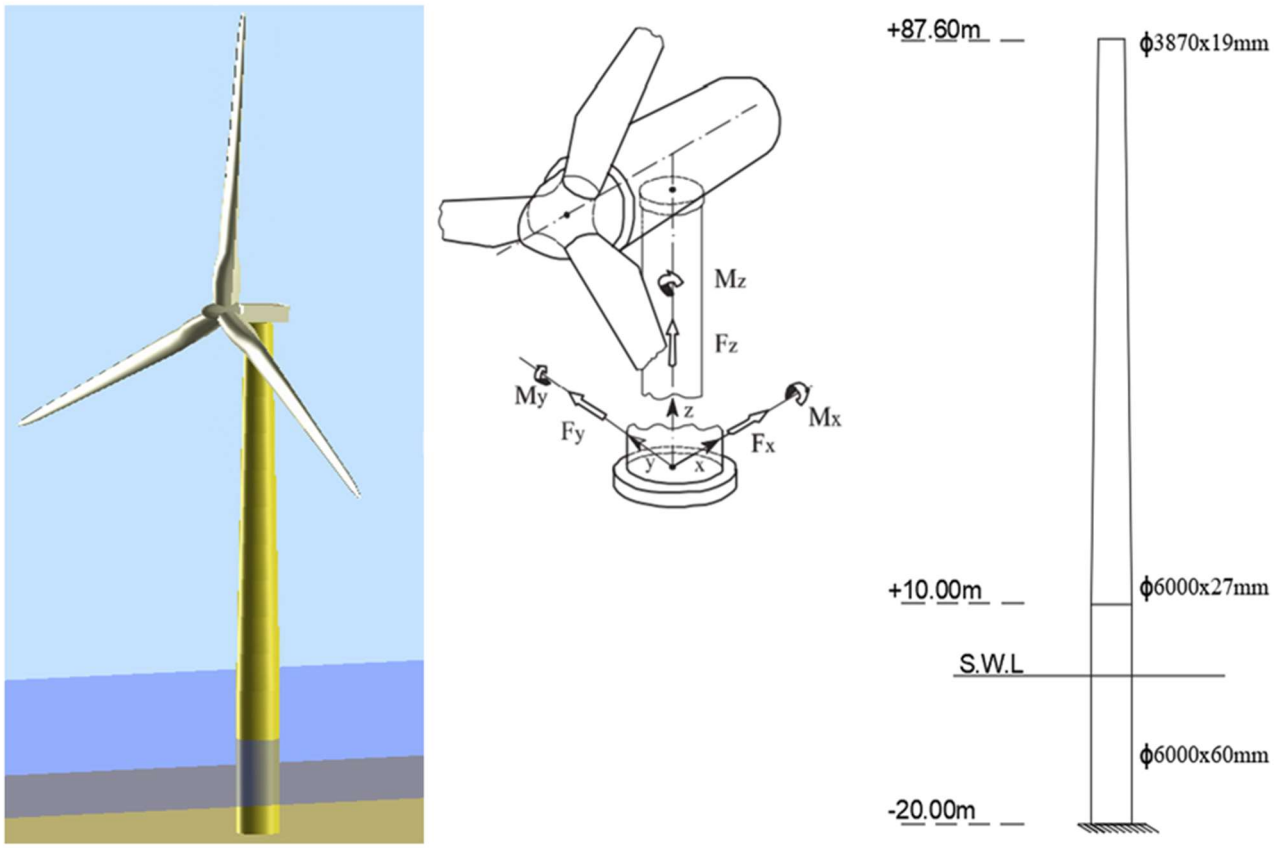

Figure 1. Test structure.

The full system is simulated in GH-BLADED [22], a software package validated by Germanischer-Lloyd for analysis and certification of offshore HAWTs. Blades, tower, nacelle, power train, as well as mechanical/electrical/control components of the turbine are modelled as described in ref. [24]. Two node,

shear-deformable Timoshenko beam elements are used for blades and tower. The model is assumed to be clamped at the seabed (-20 m).

Table 1 reports the modal frequencies obtained by GH-BLADED [22] for the parked rotor condition (one blade upward and two blades downward). They agree very well with the corresponding ones in ref. [23]. Fore-aft and side-to-side directions correspond respectively to x and y directions in Figure 1. First and second support-structure modes in fore-aft direction are reported in Figure 2.

Mode description	Frequencies (Hz)
1st support-structure side-to-side	0.2752
1st support-structure fore–aft	0.2782
1st blade asymmetric flapwise yaw	0.6833
1st blade asymmetric flapwise pitch	0.6913
1st blade collective flap	0.7210
1st blade asymmetric edgewise pitch	1.0166
1st blade asymmetric edgewise yaw	1.1032
2st blade asymmetric flapwise yaw	1.7690
2st blade asymmetric flapwise pitch	1.8624
2st blade collective flap	1.9686
2st support-structure fore-aft	2.2651
2st support-structure side-to-side	2.3452

Table 1. Modal frequencies.

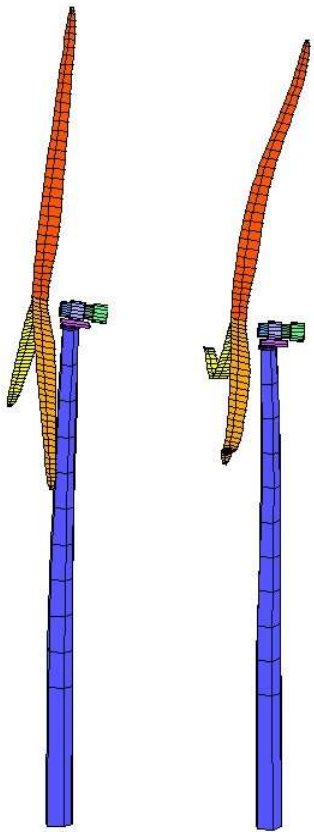

Figure 2. First and second support-structure modes in x direction.

3. AERODYNAMIC AND HYDRODYNAMIC LOADS

The Mann spectrum is used to generate the 3D turbulent wind field samples in GH-BLADED [22]. Specifically, medium turbulence fields are generated, in agreement with IEC 61400-1 [27] prescriptions for a normal turbulence model. Aerodynamic loads on the spinning rotor are generated from a dynamic wake model for the axial inflow, in conjunction with classical Blade-Element-Momentum model for tangential inflow [28]. Wind loads on the tower are included.

The JONSWAP spectrum is used to generate irregular wave samples [22]:

$$S_{JS}(f) = \alpha_2 H_S^2 T_P \left(\frac{f}{f_p}\right)^{-5} e^{-1.25(f/f_p)^{-4}} . \gamma^{\beta} \tag{1}$$

with T_p and H_S wave period and significant wave height, $fp = 1/Tp$, γ, α_2, β and δ given by [29]:

$$\gamma = \begin{cases} 5 & T_P/\sqrt{H_S} \leq 3.6 \\ e^{(5.57-1.15T_P/\sqrt{H_S})} & 3.6 \leq T_P/\sqrt{H_S} \leq 5 \\ 1 & T_P/\sqrt{H_S} \geq 5 \end{cases} \tag{2}$$

$$\alpha_2 = \frac{0.0624}{0.230+0.0336\gamma-0.185/(1.9+\gamma)}; \quad \beta = exp\left[-\frac{0.5}{\delta^2}\left(\frac{f}{f_p}-1\right)^2\right]; \quad \delta = \begin{cases} 0.07 & f \leq f_p \\ 0.09 & f > f_p \end{cases} \tag{3}$$

Hydrodynamic loads on the structural members are calculated by Morison's equation [22], with drag and inertia coefficients set according to DNV-OS-J 101 recommendations [30].

Wind and waves are assumed to be acting in the *x* direction. The equations of motion are integrated numerically, considering mutual interactions among aerodynamic and hydrodynamic responses [22], as well as the effects of the turbine active control system. The modal damping ratios are set as 0.477465% for blade modes and 1% for support-structure modes, according to the reference dataset [24]. The duration of the wind field is assumed to be 600 s, in accordance with standard procedures to simulate

normal operational conditions of wind turbines [31]-[32]-[33], extracted from a 1000-s simulation discarding the first 400 s to allow dissipation of transient behavior.

4. TUNED MASS DAMPER MODELING

The purpose of the study is to investigate the system response when a TMD is applied inside the nacelle for vibration mitigation. In GH-BLADED [22], the TMD is modeled as a lumped mass connected to the structural model by a massless spring and a viscous dashpot. Specifically, on assuming that the TMD may displace within the lower part of the nacelle (whose dimensions are 18×6×6 m, see Section 2), the TMD is connected to the tower top node of the structural model. The TMD acts simultaneously in both x and y direction.

The TMD mass is selected as percentage of the total mass. Three different mass ratios are selected, 1%, 2% and 5%, as in similar studies [4]-[5]-[7]. TMD damping ratio is set equal to 5%.

TMD performances will be assessed for various wind velocities at the hub, in both operational (spinning) and parked rotor state: V=5 m/s, 11.4 m/s (rated speed), 15 m/s, 20 m/s, 24 m/s in operational state (cut-out speed of the turbine = 25 m/s, i.e.); V=30 m/s, 35 m/s, 40 m/s in parked state. A typical ocean sea state is considered, with T_p = 10 s and H_s = 6 m , in agreement with ref. [23].

For a preliminary insight, Section 5 will discuss the dynamics of the system without TMD. Next, Section 6 will assess the response of the system with TMD, estimating standard deviation of tower top displacement, TMD displacements as well as power production.

5. SYSTEM DYNAMICS WITHOUT TMD

It is of interest to investigate the dynamics of the system without TMD in both fore-aft and side-to-side directions, as shown next.

5.1. Fore-aft response without TMD

First, the operational rotor state is considered. The Fourier Transforms (FTs) of tower top displacement Dx, out-of-plane aerodynamic loading at blade half length, rotor angular speed, shear force Fx and bending moment My at the tower top, are calculated for wind + wave and wind only, and reported in Figure 3 through Figure 7. Notice that the FT of the out-of-plane aerodynamic loading at blade half length, shown in Figures 3-7, may reasonably be taken as representative of the FTs of the out-of-plane aerodynamic loading along the whole blade, as indeed the numerical simulations in GH-BLADED [22] show that the main frequency content of the out-of-plane aerodynamic loading falls within similar frequency ranges at various stations along the blade (e.g., see [12]-[13]). Some examples are reported in Appendix A for completeness.

Comparing the FTs of the tower top displacement Dx, shear force Fx and bending moment My in Figures 3-7, suggests two relevant observations:

(i) In general, peaks and main frequency contents in the FT of Dx are present in the FTs of out-of-plane aerodynamic loading and/or rotor speed. Recognize that the frequency content slightly above 0.3 Hz for V=5 m/s and around 0.25 Hz for V=15 m/s is also in the FT of the corresponding rotor speed, the peak at 0.16 Hz for V=20 m/s and V=24 m/s is present in the FT of the corresponding out-of-plane aerodynamic loading as well as rotor speed and, likewise, the frequency content at about 0.31 Hz for V=20 m/s and V=24 m/s is visible in the FT of the corresponding out-of-plane aerodynamic loading. This agrees with the fact that the part of the system above the tower top is acted upon by aerodynamic loading as well as inertial forces associated with rotor dynamics, which are generally dependent on rotor speed. A further observation is that, for all wind velocities, the FT of Dx exhibits a significant frequency content close to zero frequency. This is especially true for the rated speed V=11.4 m/s where no other relevant peaks are seen in the FT, meaning that the tower top displacement Dx has almost constant value and very small oscillatory part. This is evidence that the control system of the HAWT minimizes tower oscillations at the rated speed.

(ii) In some cases, peaks and main frequency contents in the FT of the out-of-plane aerodynamic loading are not present in the FT of the tower top displacement Dx. For instance, recognize that the peaks at 0.12 Hz and 0.24 Hz for V=5 m/s, the frequency content around 0.2 Hz and slightly above 0.4 Hz for V=11.4 m/s, as well as at the peaks at 0.2 Hz and 0.43 Hz for V=15 m/s, are in the FT of the out-of-plane aerodynamic loading but are not present in the FT of Dx.

Now, in order to substantiate observation (ii), i.e. that the FT of the tower top displacement Dx contains only some of the peaks and main frequency content of the out-of-plane aerodynamic loading, attention is focused on the FT of the shear force Fx and bending moment My at the tower top, reported in Figures 3-7. The FTs of these quantities suggest the following comments.

The first comment is that all peaks and main frequency content in the FT of Dx are present indeed in the FT of Fx and/or My at the tower top. This result is expected, in recognition of the fact that the tower behaves linearly. Hence, the FT of Dx reflects the FT of Fx and/or My, as modulated by the transfer function of the tower. This is apparent in Figures 3-7, where the frequency content of Dx is essentially governed by the frequency content of Fx and/or My closer to the natural frequency 0.2782 Hz of the first fore-aft support structure mode (Table 2), with negligible contributions from that away from 0.2782 Hz (e.g., the frequency content of My slightly above 0.6 Hz, for V=15 m/s).

The second comment substantiates observation (ii). It is seen indeed that the peaks at 0.12 Hz and 0.24 Hz for V=5 m/s, which are present in the FT of the out-of-plane aerodynamic loading, are not present in the FT of the corresponding Dx because they are not present in neither the FT of Fx nor the FT of My. The same holds true for the frequency content in the FT of the out-of-plane aerodynamic loading around 0.2 Hz and slightly above 0.4 Hz for V=11.4 m/s, as well as the peak at 0.2 Hz for V=15 m/s, which are not present in the FT of Fx and My and, consequently, are not present in the FT of Dx. An explanation to the fact that the FTs of Fx and My do not reflect the FT of the out-of-plane aerodynamic loading may be given considering that, in the operational state, the dynamics of the rotor is non-linear. There are various sources of non-linearity: e.g., aerodynamic lift/drag forces depend non-linearly on the wind speed relative

to the blades, to which contribute rotor angular speed and blade oscillation; on the other hand, rotor angular speed and blade oscillation are affected by tower top motion that, in turn, is caused by aerodynamic lift/drag forces as well as inertial forces associated with rotor dynamics. In addition, in the operational state the dynamics of the rotor is influenced by the active control system that changes the pitch angle of the blades. All these issues are relevant to explain the fact that, in some cases, peaks and main frequency content in the FT of the out-of-plane aerodynamic loading may not be present in the FT of the shear force Fx and bending moment My and, in turn, in the FT of the tower top displacement Dx, as pointed out in observation (ii). Clear evidence of non-linearity is, for instance, the frequency content around 0.6 Hz for V=11.4 m/s, which is present in the FT of Fx but not in the out-of-plane aerodynamic loading.

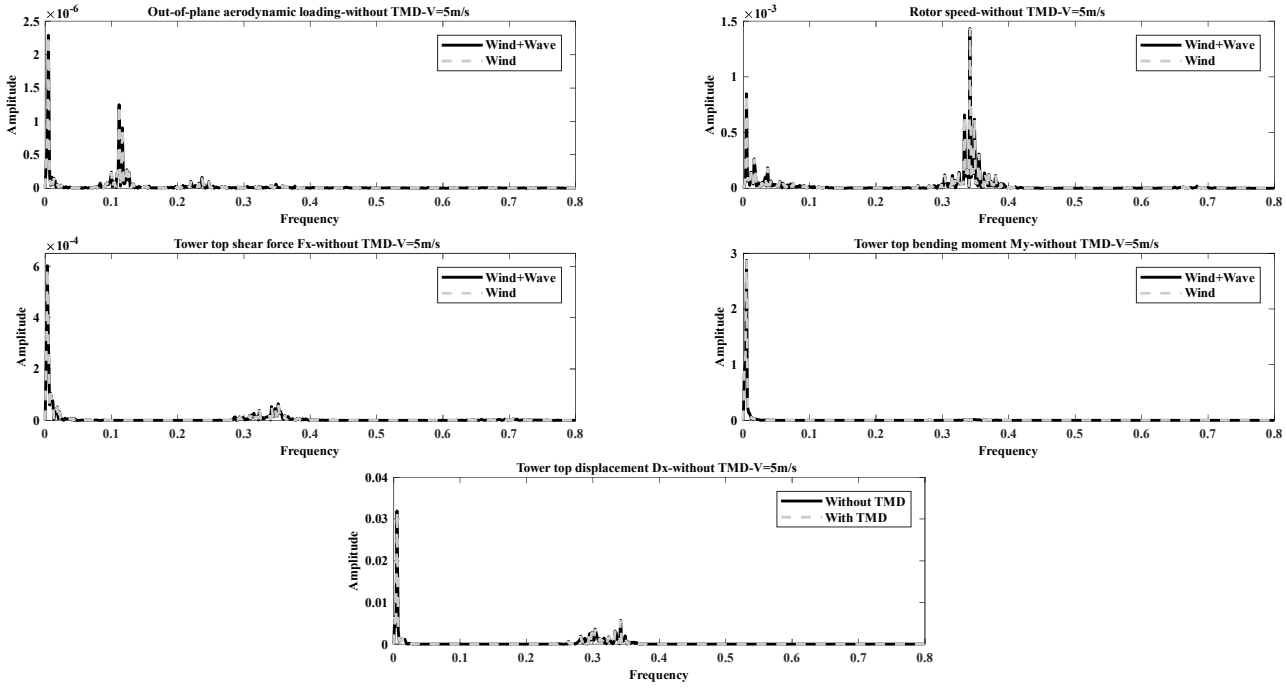

Figure 3. Fourier Transforms of response variables in *x* direction, for V=5 m/s.

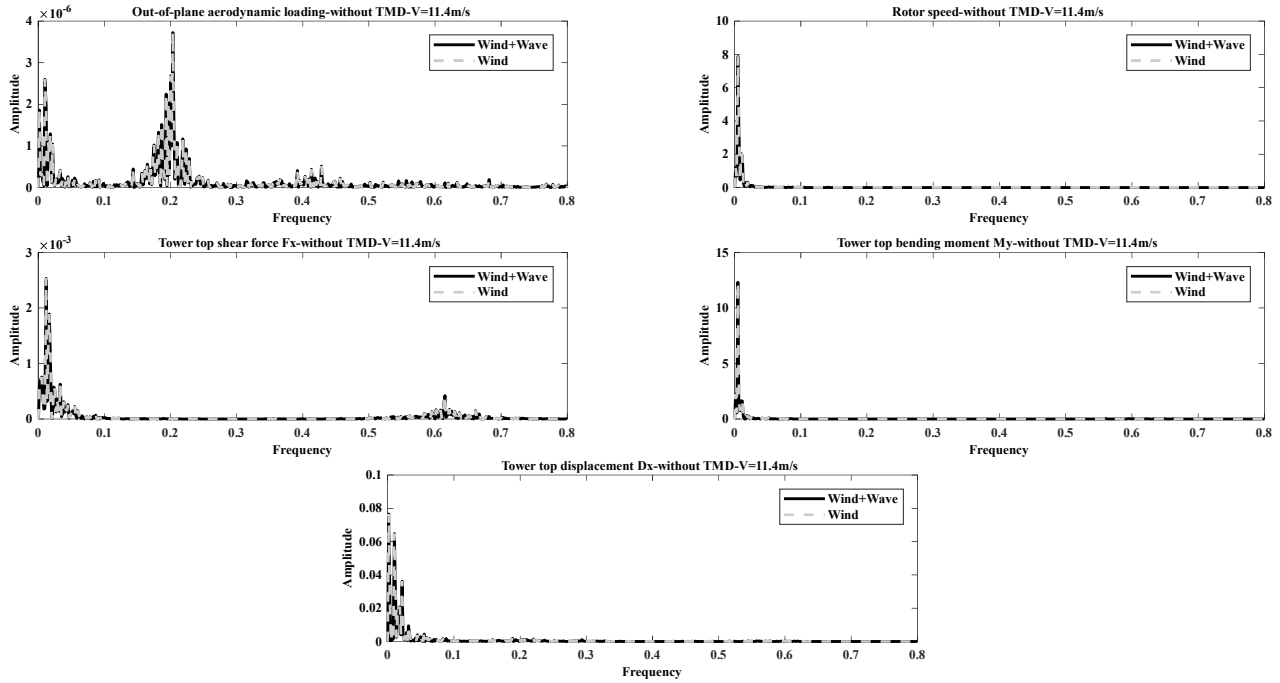

Figure 4. Fourier Transforms of response variables in *x* direction, for V=11.4 m/s.

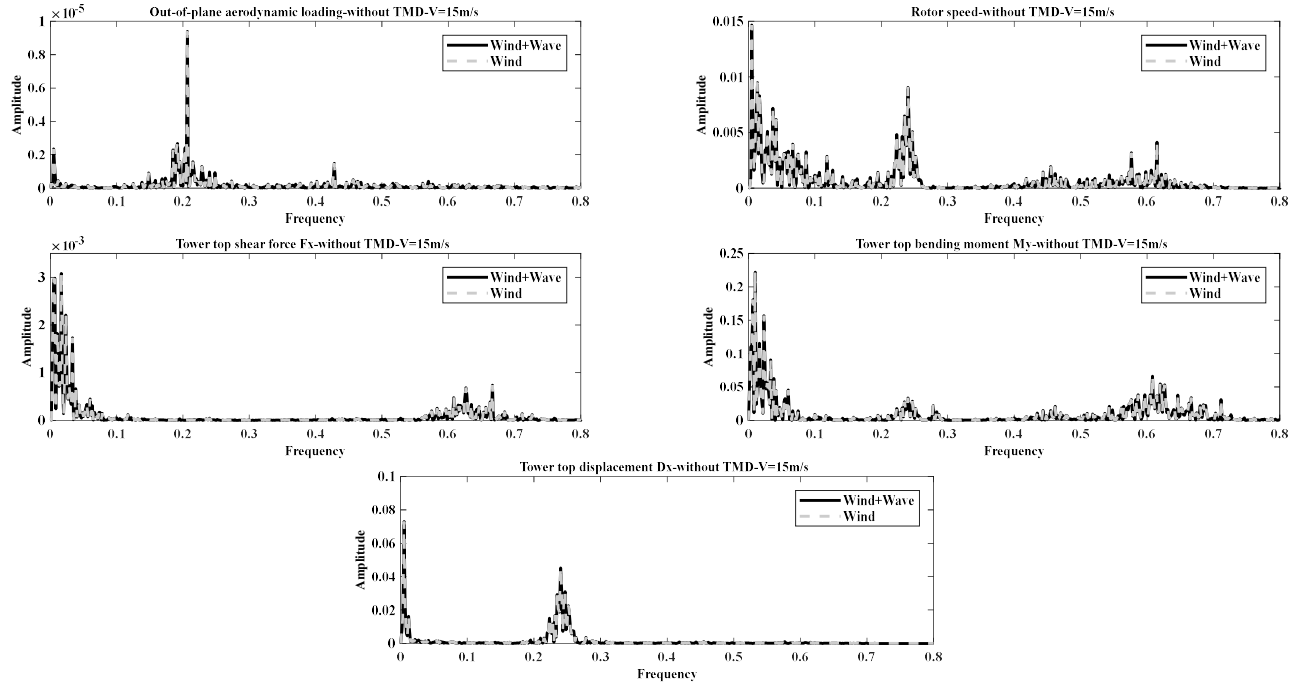

Figure 5. Fourier Transforms of response variables in *x* direction, for V=15 m/s.

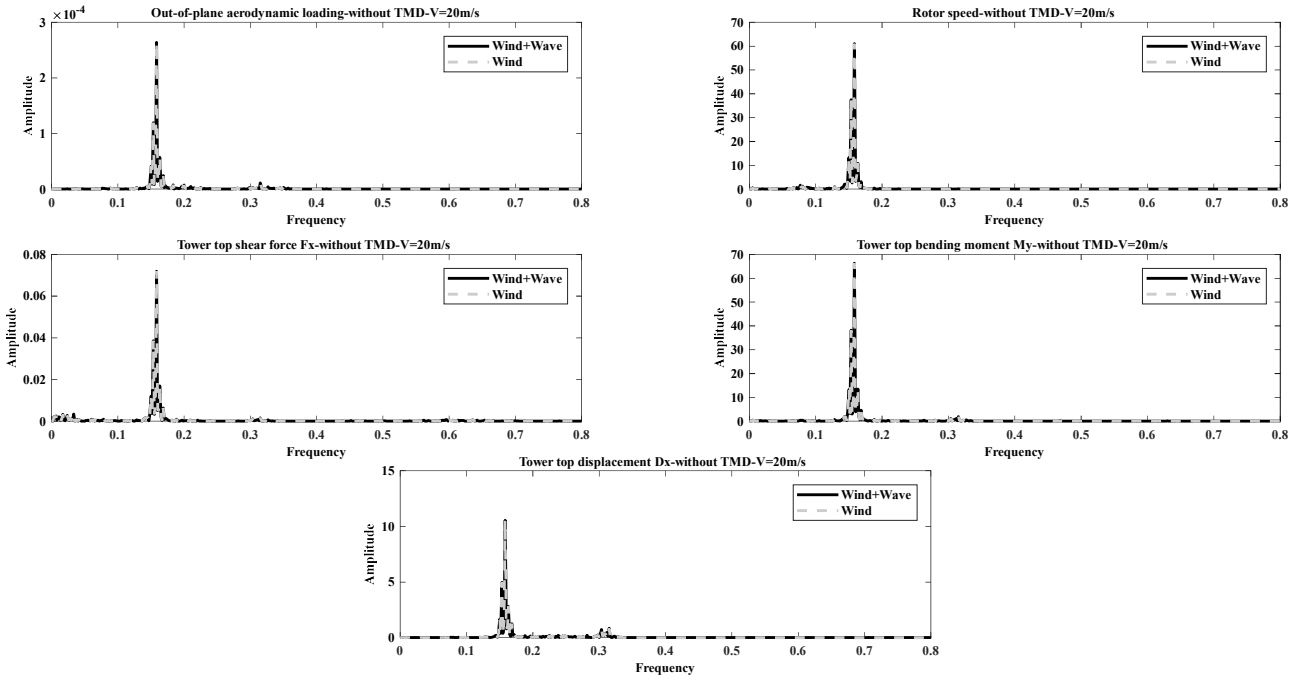

Figure 6. Fourier Transforms of response variables in *x* direction, for V=20 m/s.

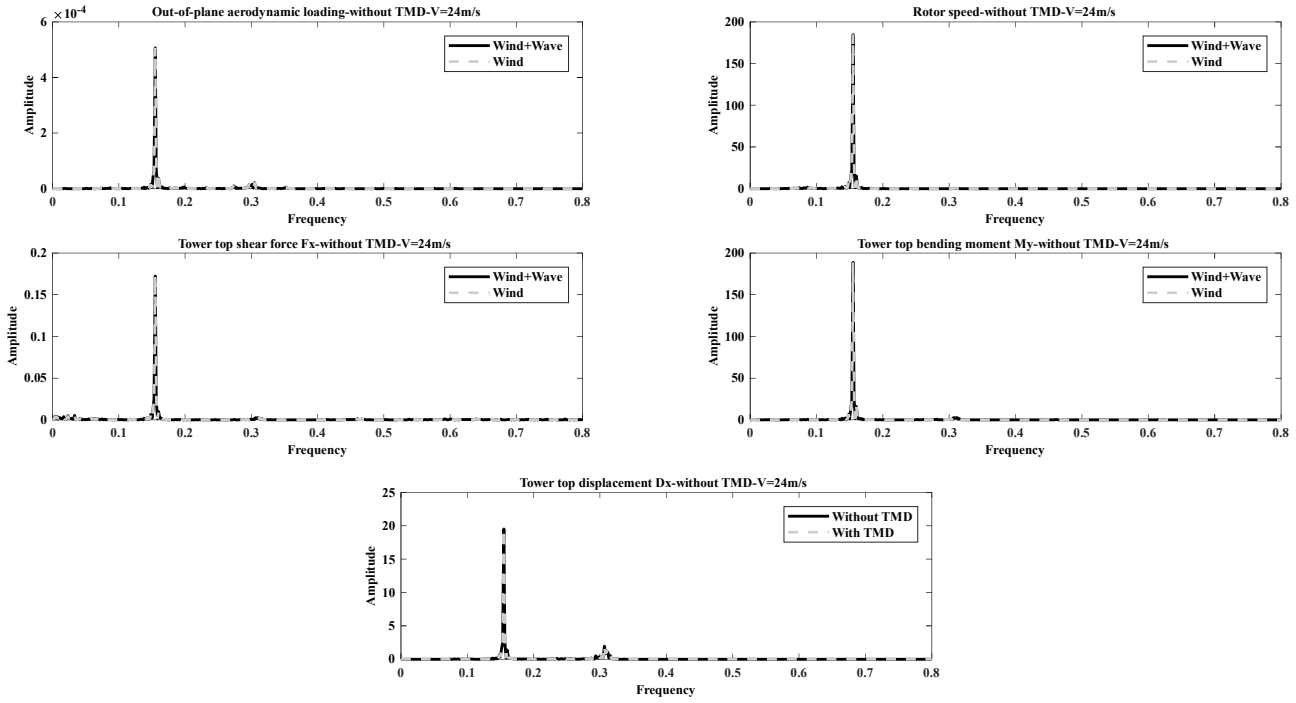

Figure 7. Fourier Transforms of response variables in *x* direction, for V=24 m/s.

After discussing the essential features of system dynamics in operational conditions, next a rotor parked state is considered for wind velocities exceeding the cut-out speed of the turbine = 25 m/s, namely V=30 m/s, 35 m/s, 40 m/s. Specifically, FTs of tower top displacement Dx, out-of-plane aerodynamic loading at blade half length, shear force Fx and bending moment My at the tower top, are calculated for wind + wave and wind only, and are reported in Figure 8 through Figure 10. In all these cases, it is evident that the FT of Dx is well centered about the natural frequency of the first fore-aft support-structure mode, i.e. 0.2782 Hz (see Table 1). In addition, the FTs of both Fx and My generally reflect the FT of out-of-plane aerodynamic loading. These observations show that in a rotor parked state the system behavior is quite close to a linear one, with a response dominated essentially by the first fore-aft support structure mode. That is, in a rotor parked state, non-linear dependence of aerodynamic lift/drag forces on blade oscillation does not seem to play a significant role.

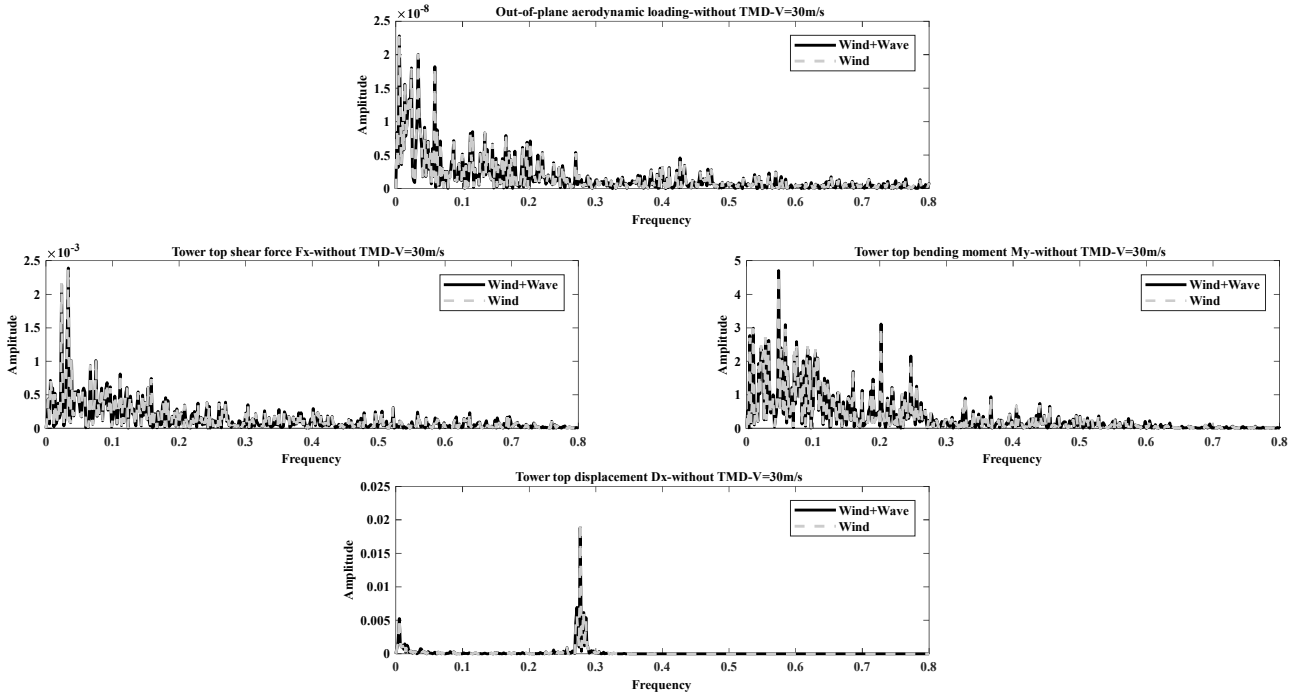

Figure 8. Fourier Transforms of response variables in *x* direction, for V=30 m/s.

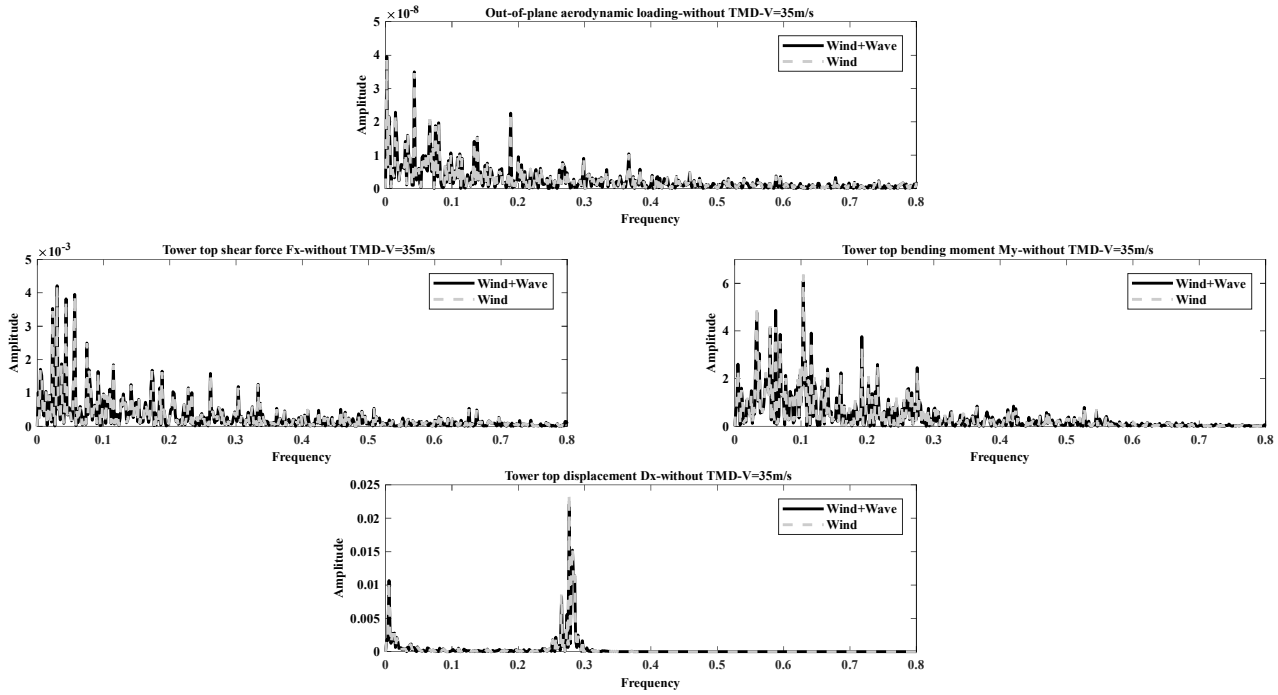

Figure 9. Fourier Transforms of response variables in *x* direction, for V=35 m/s.

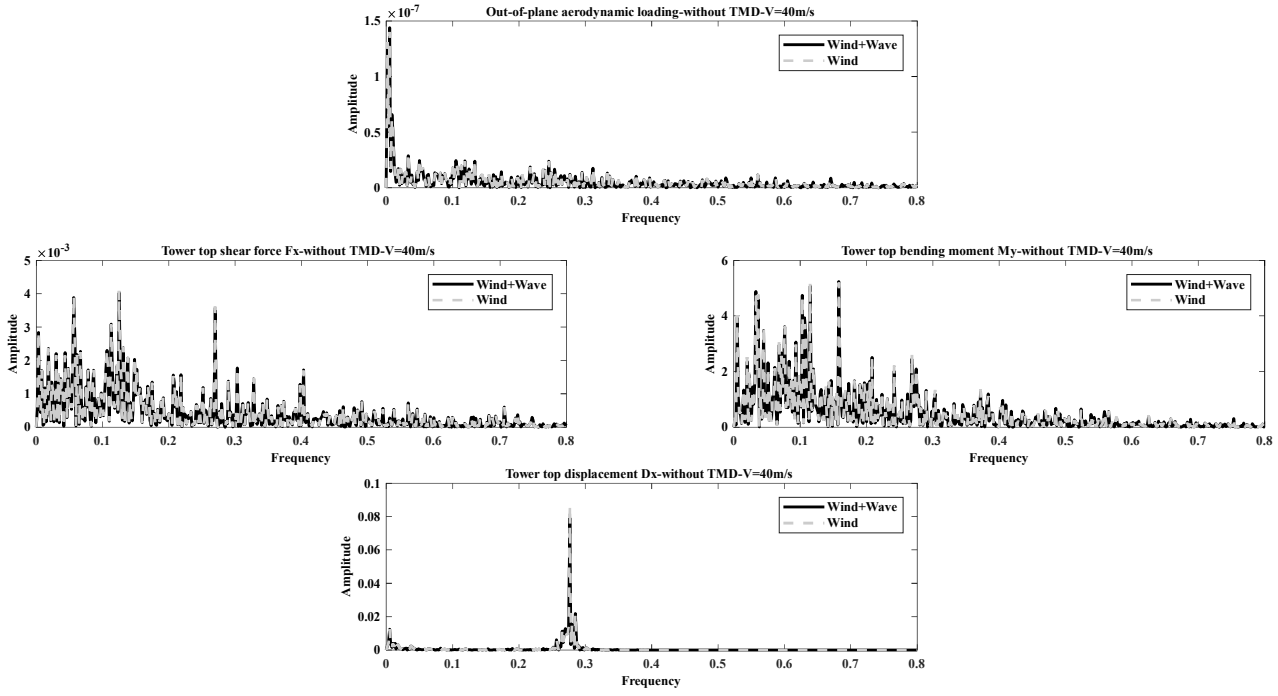

Figure 10. Fourier Transforms of response variables in *x* direction, for V=40 m/s.

5.2. Side-to-side response without TMD

Next, for a further insight into the dynamics of the system without TMD, the response in *y* direction is investigated, for the same operational and parked rotor states in Figures 3-10.

Figures 11-15 report the FTs of tower top displacement Dy, as well as in-plane aerodynamic loading at blade half length, rotor angular speed, shear force Fy and bending moment Mx at tower top for the operational wind velocities. Again, the FT of the in-plane aerodynamic loading at blade half length can be taken as representative of the FTs along the whole blade, based on evidence from numerical simulations in GH-BLADED [22] and in accordance with previous studies [12]-[13].

Comments on Figures 11-15 mirror those on Figure 3-7. In general, peaks and main frequency contents in the FT of Dy are present also in the FTs of the in-plane aerodynamic loading and/or rotor speed. Considering linear behavior of the tower, they can be obtained from the FTs of Fy and Mx through the transfer function of the tower, which has a peak at the natural frequency 0.2752 Hz of the first side-to-side support-structure mode (see again Table 2). Indeed, the FT of Dy generally exhibits a peak at 0.2752 Hz for all wind velocities. It is also seen that some peaks and main frequency contents in the FTs of the in-plane aerodynamic loading and rotor speed are not present in the FT of the tower top displacement Dy. Again, as in Figures 3-7, this happens for those peaks and main frequency contents which are not present in the FTs of Fy and My, see for instance peaks at 0.12 Hz for V=5 m/s or 0.2 Hz for V=11.4 m/s.

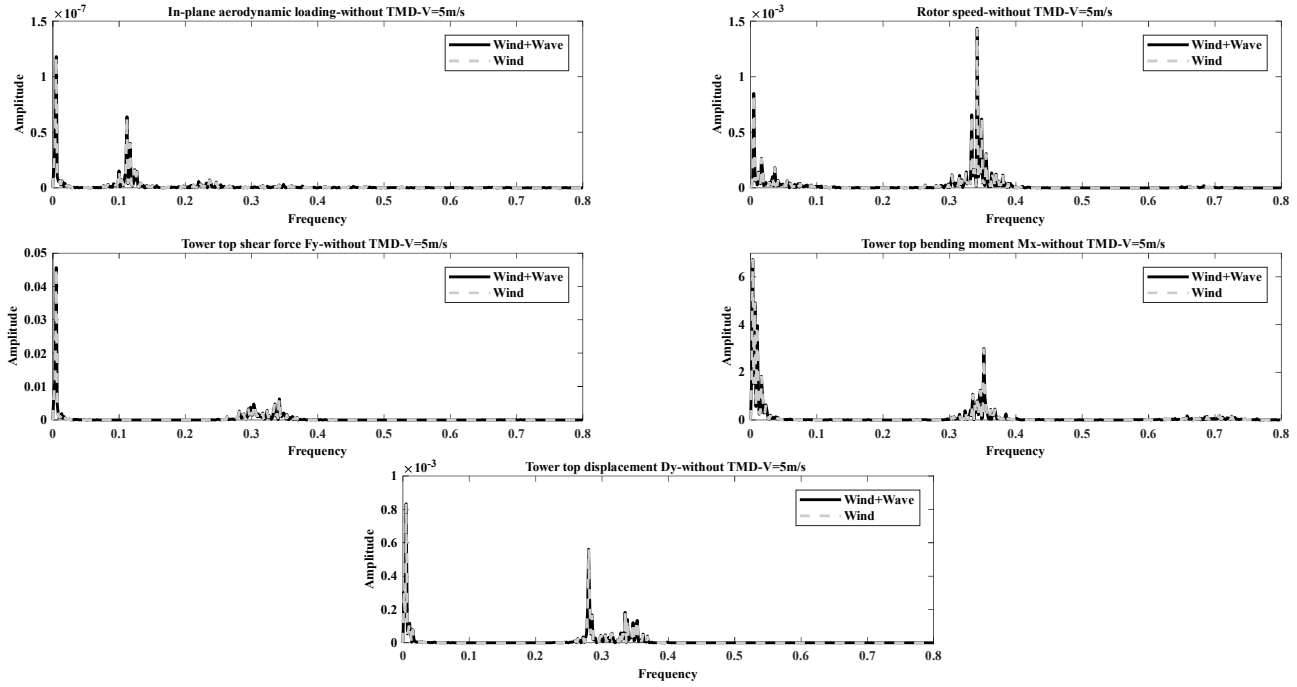

Figure 11. Fourier Transforms of response variables in *y* direction, for V=5 m/s.

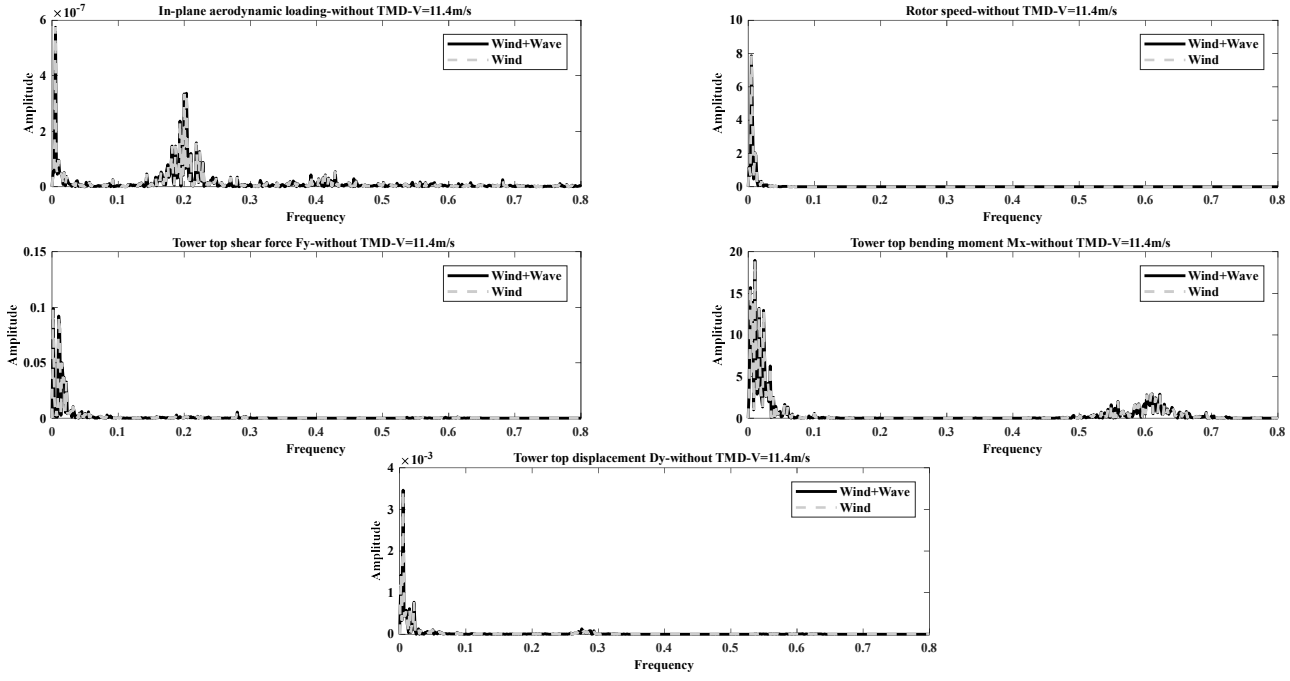

Figure 12. Fourier Transforms of response variables in *y* direction, for V=11.4 m/s.

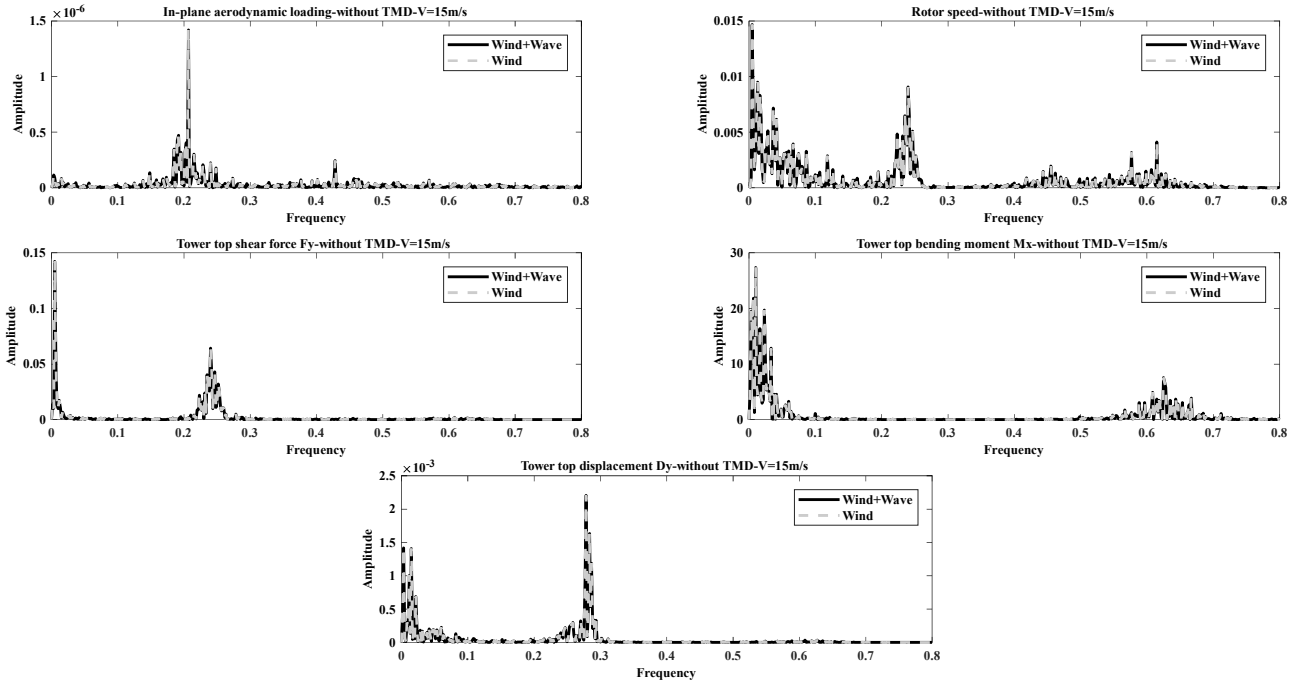

Figure 13. Fourier Transforms of response variables in *y* direction, for V=15 m/s.

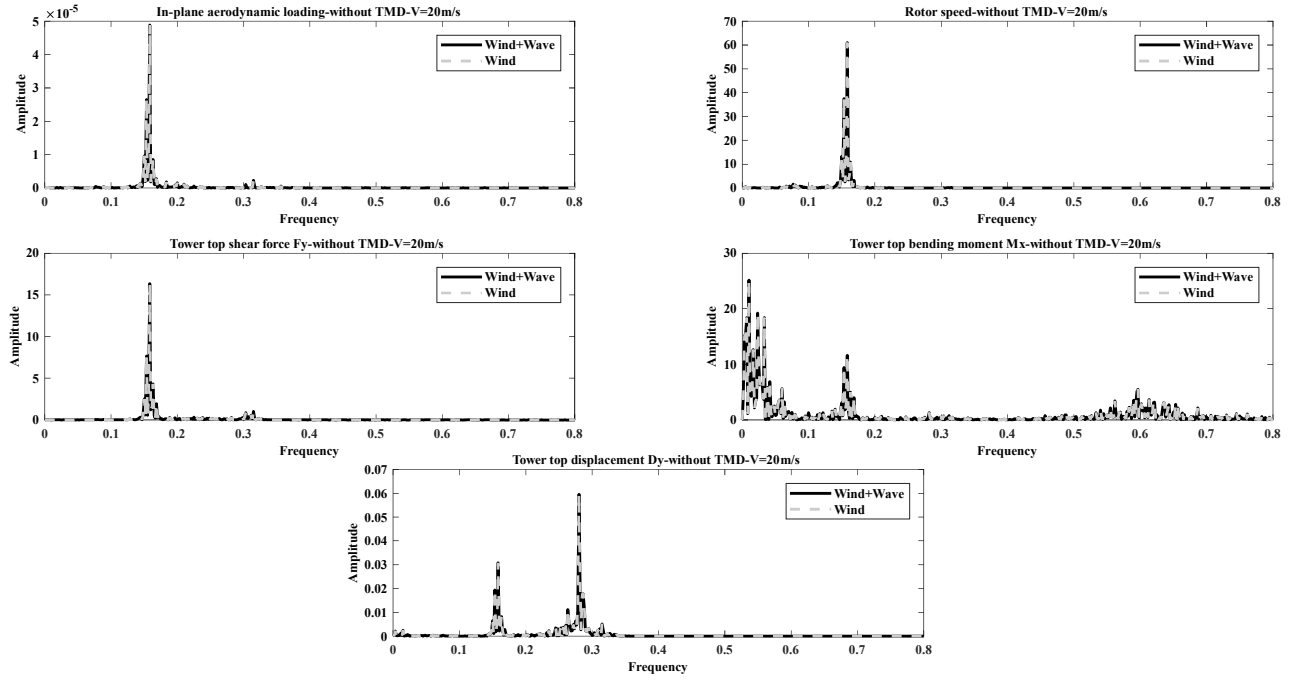

Figure 14. Fourier Transforms of response variables in *y* direction for V=20 m/s.

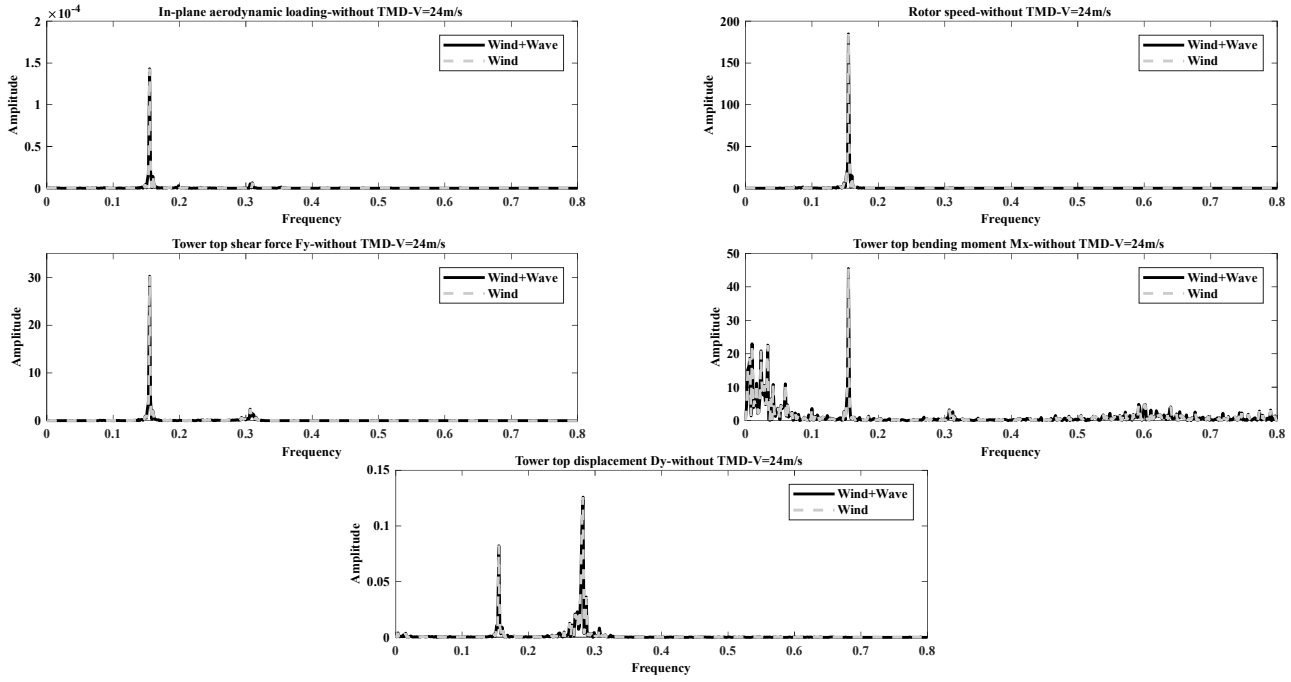

Figure 15. Fourier Transforms of response variables in *y* direction for V=24 m/s.

Figures 16-18 show the FTs of tower top displacement Dy, in-plane aerodynamic loading at blade half length, shear force Fy and bending moment My at tower top, for the rotor parked states considered in Figures 8-10. Results appear consistent with corresponding ones for *x* direction shown in Figures 8-10, i.e. the system behavior is close to a linear one. The FT of Dy has a peak at about 0.2752 Hz, i.e. the natural frequency of the first side-to-side support-structure mode, while the FTs of Fy and Mx reflect the FT of in-plane aerodynamic loading; especially the FT of Fy appears to be dominated by the first side-to-side support-structure mode.

A final general comment on Figures 11-18 is that amplitudes of the tower top displacement Dy are well smaller than corresponding ones in the tower top displacement Dx, shown in Figures 3-10. This is expected considering that wind loads in *x* direction cause the tower to oscillate more in fore-aft direction than in side-to-side one.

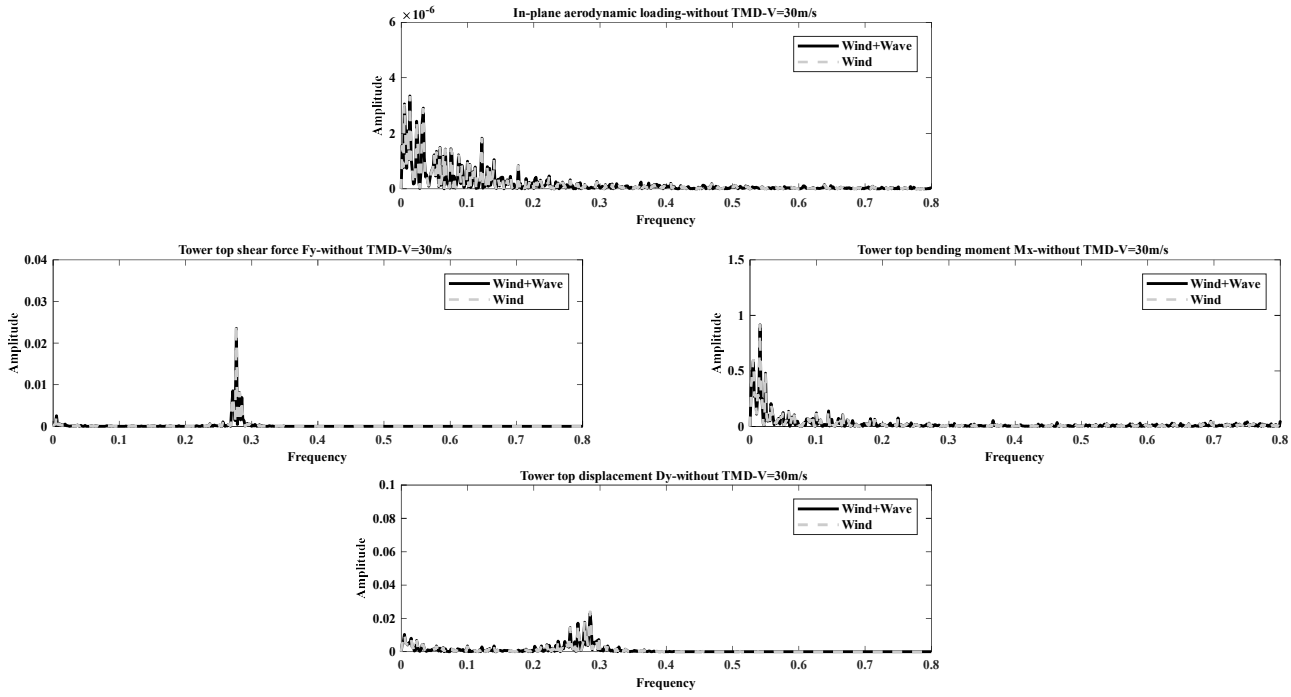

Figure 16. Fourier Transforms of response variables in *y* direction, for V=30 m/s.

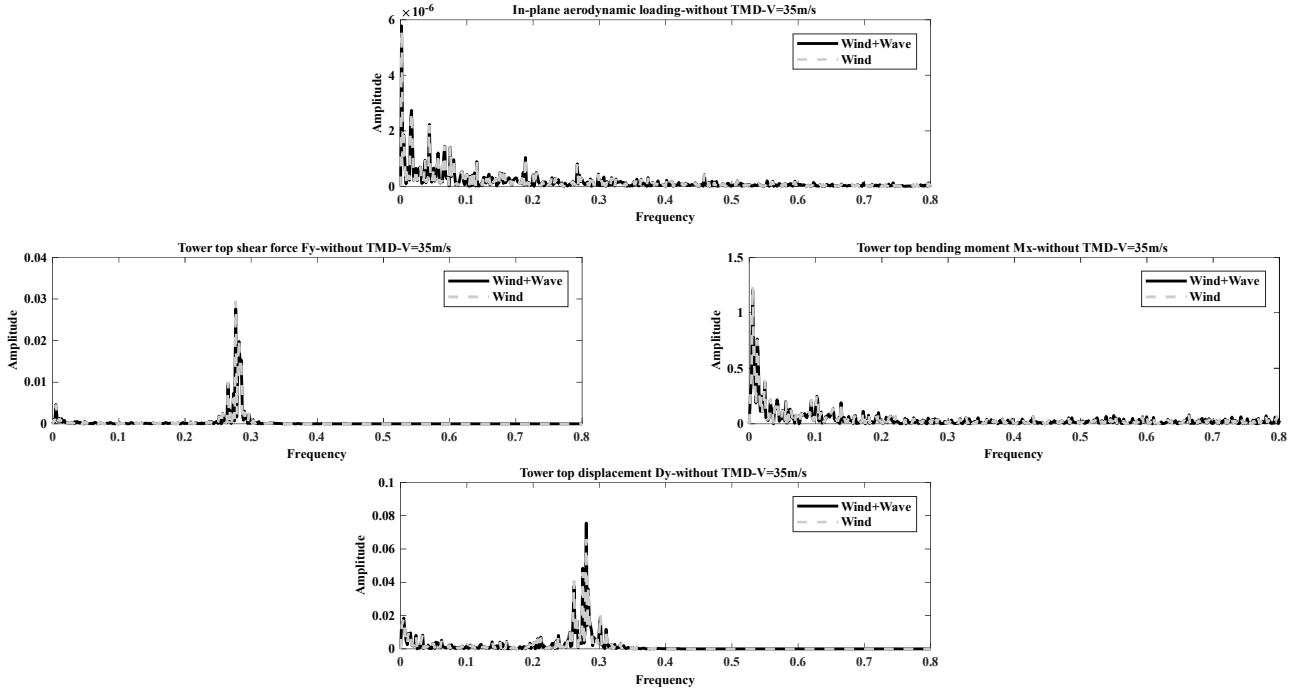

Figure 17. Fourier Transforms of response variables in *y* direction, for V=35 m/s.

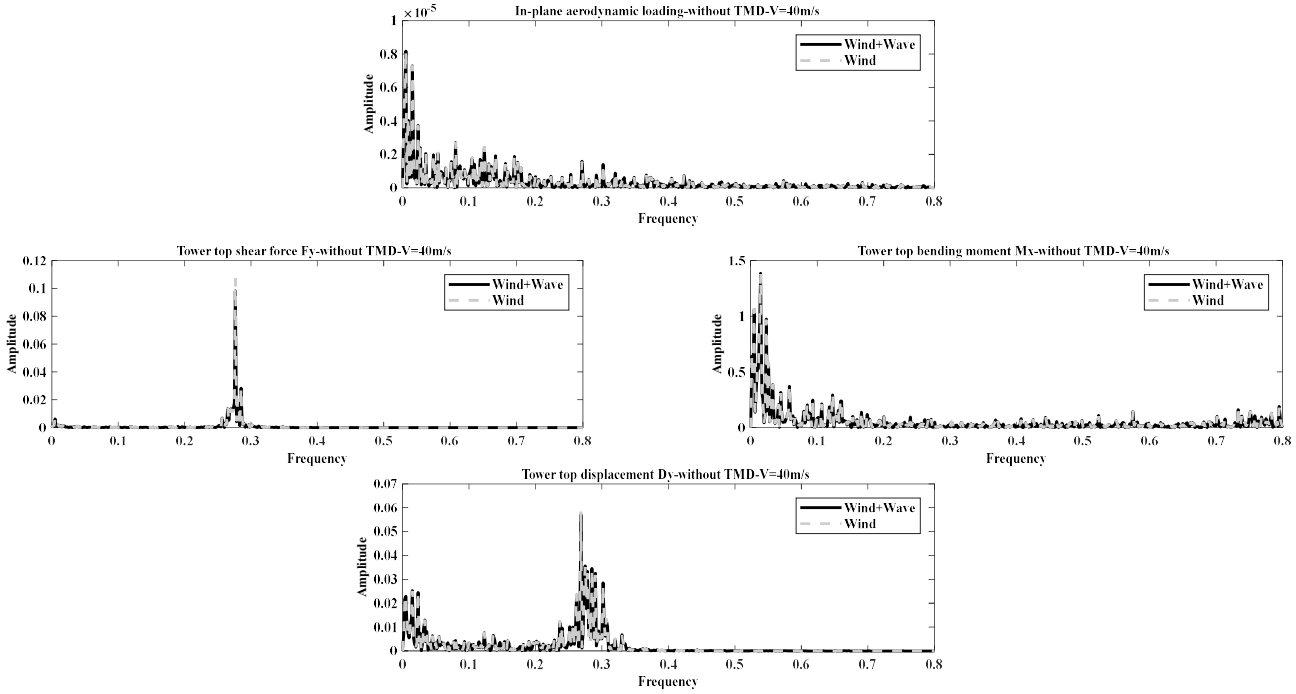

Figure 18. Fourier Transforms of response variables in *y* direction, for V=40 m/s.

5.3. Remarks on system dynamics without TMD

At this point, with the purpose of driving the investigations on the system dynamics with TMD, to be discussed in the next Section, the essential information drawn from Figures 3-18 can be summarized as follows.

Regarding the operational rotor state, Figures 3-7 and Figures 11-15 have shown that, in general, peaks and main frequency contents in the FT of tower top displacements Dx and Dy are present in the FTs of corresponding aerodynamic loading and/or rotor speed. It has been also noticed, however, that the system response is inherently non-linear. Because of non-linearity, in the next Section various potential tuning frequencies will be explored for the TMD. In general, it is expected that the TMD will be effective when capable of reducing those peaks and main frequency contents in the FTs of aerodynamic loading and/or rotor speed that are also present in the FT of the tower top displacement, as shown in Figures 3-7 and Figures 11-15. Not only various tuning frequencies but also various mass ratios will be considered for the TMD.

As for the parked rotor state, Figures 8-10 and Figures 16-18 have shown that the system behavior can approximately be taken as linear. In view of linearity, it may be expected that best TMD performances will be attained at a tuning frequency close to the natural frequency of first support-structure modes in fore-aft and side-to-side directions. This will be assessed in the next Section, taking for comparison various potential tuning frequencies. Namely, the tuning frequencies as well as the mass ratios considered for the operational rotor state will be considered also for the parked rotor state.

The final remark on Figures 3-18 is that results for wind + wave are practically coincident with those for wind only, for all the considered wind velocities. The fact that wave loading has little effect substantiate the statement above, i.e. that the TMD will be effective when capable of reducing peaks and main frequency contents in the FTs of aerodynamic loading and/or rotor speed and, specifically, those which are also present in the FT of the tower top displacement.

6. SYSTEM DYNAMICS WITH TMD

Here, TMD tuning frequencies are selected as to encompass the frequency range of interest in Figures 3-18, i.e. approximately from 0.16 Hz to 0.35 Hz, with specific values targeting the relevant frequency content of the tower top displacements Dx and Dy as well as the natural frequencies of the first fore-aft and side-to-side support-structure modes, i.e. 0.2782 Hz and 0.2752 Hz. For both, the tuning frequency is approximated to 0.28 Hz. System dynamics with TMD is studied for the wind velocities and sea state considered in Section 5.

6.1. Fore-aft response with TMD

Tables 2 reports the standard deviation of the tower top displacement Dx for the various tuning frequencies and mass ratios of the TMD, as well as all wind velocities.

Regarding the operational rotor state in Table 2, a first important observation is that results obtained for the rated wind speed V=11.4 m/s differ significantly from those obtained for the other operational velocities. For V=11.4 m/s, the TMD provides no reduction in the standard deviation of Dx, irrespective

of tuning frequency and mass ratio (reductions are indicated by negative values). For the other operational velocities, the TMD provides a reduction in the standard deviation of Dx, with maximum reduction at different tuning frequencies: 0.35 Hz for V=5 m/s, 0.24 Hz for V=15 m/s, 0.31 Hz for V=24 m/s, with any mass ratio; 0.24 Hz with 1% mass ratio and 0.28 Hz with 2% and 5% mass ratios for V=20 m/s. Maxima reductions are not the same for all wind velocities, i.e. about -20% for V=5 m/s, -25% for V=15 m/s, -79% for V=20 m/s, -7% for V=24 m/s. In general, they are obtained with the largest mass ratio, i.e. 5%, except for V=24 m/s where the maximum reduction -7.34% is obtained with 2% mass ratio. To understand these results, the following considerations can be made.

Standard Deviation Changes (%)-D_x									
Mass ratio	**Frequency (Hz)**	**Wind speed (m/s)**							
		V=5	**V=11.4**	**V=15**	**V=20**	**V=24**	**V=30**	**V=35**	**V=40**
1%	**0.16**	+0.7685	-0.1886	-13.9289	+1.4243	+3.1119	-2.4424	-0.031	-3.8574
	0.2	+1.1196	-0.1901	-21.8380	+1.7372	+1.6043	-5.1849	-1.3131	-8.3712
	0.24	+1.2938	+0.1411	-23.2551	-36.3316	-0.0113	-15.9160	-9.8052	-19.5193
	0.28	-0.2377	+0.2510	-8.4553	-0.6641	-0.9072	-30.6995	-24.6625	-29.6998
	0.31	-5.2359	+0.1737	+9.2523	-0.2423	-5.9295	-18.1584	-15.4395	-10.8789
	0.35	-8.9846	+0.3044	+15.2744	-0.0072	-3.3179	-7.3369	-10.1609	-1.8126
2%	**0.16**	+1.5149	-0.2732	-19.8877	+0.5271	+6.3465	-4.3331	-0.1623	-8.2483
	0.2	+2.2254	-0.2227	-24.9851	+3.3938	+3.1319	-9.9568	-3.2278	-13.8258
	0.24	+2.7396	+0.3995	-25.1738	-45.0873	+1.6391	-24.7338	-18.7843	-27.8417
	0.28	+0.2018	+0.3564	-15.0365	-67.8895	+0.9819	-31.9352	-27.6274	-33.5252
	0.31	-6.2173	+0.3831	-1.5073	+2.4762	-7.3441	-26.2051	-15.6377	-16.6784
	0.35	-14.1071	+0.4678	+10.0833	+0.3752	-3.9389	-14.8738	-8.0624	-2.7096
5%	**0.16**	+3.7459	-0.5019	-24.2338	-5.0031	+8.6861	-10.9699	-3.7769	-14.8995
	0.2	+5.5013	+0.0594	-24.4986	+11.6573	+8.5151	-22.4947	-15.6807	-24.7366
	0.24	+6.0929	+1.3231	-25.7926	-79.6744	+5.0488	-32.8322	-29.4657	-35.432
	0.28	+1.8771	+1.3810	-13.9125	-79.8730	+0.7136	-29.0379	-30.4613	-37.4314
	0.31	-10.1346	+1.1924	+16.6118	-18.9526	-6.6894	-25.2694	-18.8798	-26.6805
	0.35	-20.8415	+1.3380	+7.3770	+3.6253	-4.5931	-18.2842	-7.5228	-7.6913

Table 2. Variations in standard deviation of tower top displacement Dx after TMD application.

The explanation to the TMD behavior for V=11.4 m/s is straightforward based on the FTs in Figure 4, which shows that the tower top displacement Dx has almost constant value (all relevant frequency content is close to zero frequency) and negligible oscillation (no relevant frequency content above zero). Since the system does not vibrate significantly, the TMD is practically inactive at any tuning frequency and mass ratio.

To gain insight into the reasons why, for the other operational wind velocities, the TMD performs well at some tuning frequencies but is not effective at some others, the FTs of the tower top displacement Dx, out-of-plane aerodynamic loading at half blade length and rotor angular speed, with and without TMD, are reported in Figure 19 through Figure 24, for some typical cases.

Figure 19 shows the case V=5 m/s with TMD tuning frequency = 0.35 Hz, when reductions progressively increase with mass ratio, i.e. from -8.98% with 1% mass ratio to -20.84% with 5% mass ratio, see Table 2. It is apparent that, in this case, the presence of the TMD changes and reduces the frequency content in the FT of the rotor speed, with a consequent reduction of the frequency content in the FT of Dx. Figures 20-24 report other cases in which the TMD is effective and, specifically: V=15 m/s for TMD tuning frequencies 0.20 Hz, 0.24 Hz and 0.28 Hz, V=20 m/s for TMD tuning frequencies 0.24 Hz and 0.28 Hz. In all these cases, the presence of the TMD affects and reduces the frequency content in the FT of either the out-of-plane aerodynamic loading or the rotor speed, with a consequent reduction of the frequency content in the FT of Dx.

Scenarios in which the TMD is not effective are reported in Figures 25-26, which refer to V=15 m/s for TMD tuning frequency 0.35 Hz and V=5 m/s for TMD tuning frequency 0.24 Hz (see variations in Dx standard deviation, Table 2). In these cases, the presence of the TMD does not change the frequency content in the FT of neither the out-of-plane aerodynamic loading nor the rotor speed, and this explains why no reductions of the frequency content in the FT of Dx are obtained.

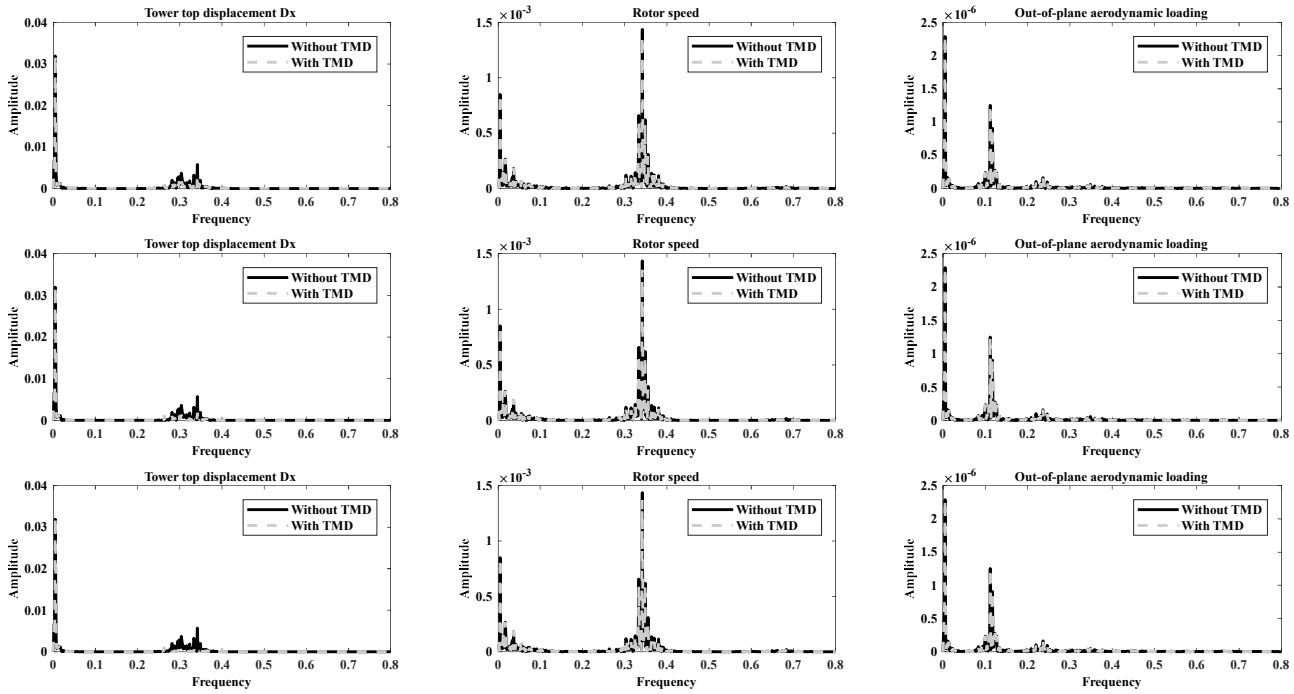

Figure 19. Fourier Transforms of tower top displacement Dx, rotor speed and out-of-plane aerodynamic loading without and with TMD for V=5 m/s, tuning frequency=0.35 Hz; mass ratios: 1% (1st row), 2% (2nd row), 5% (3rd row).

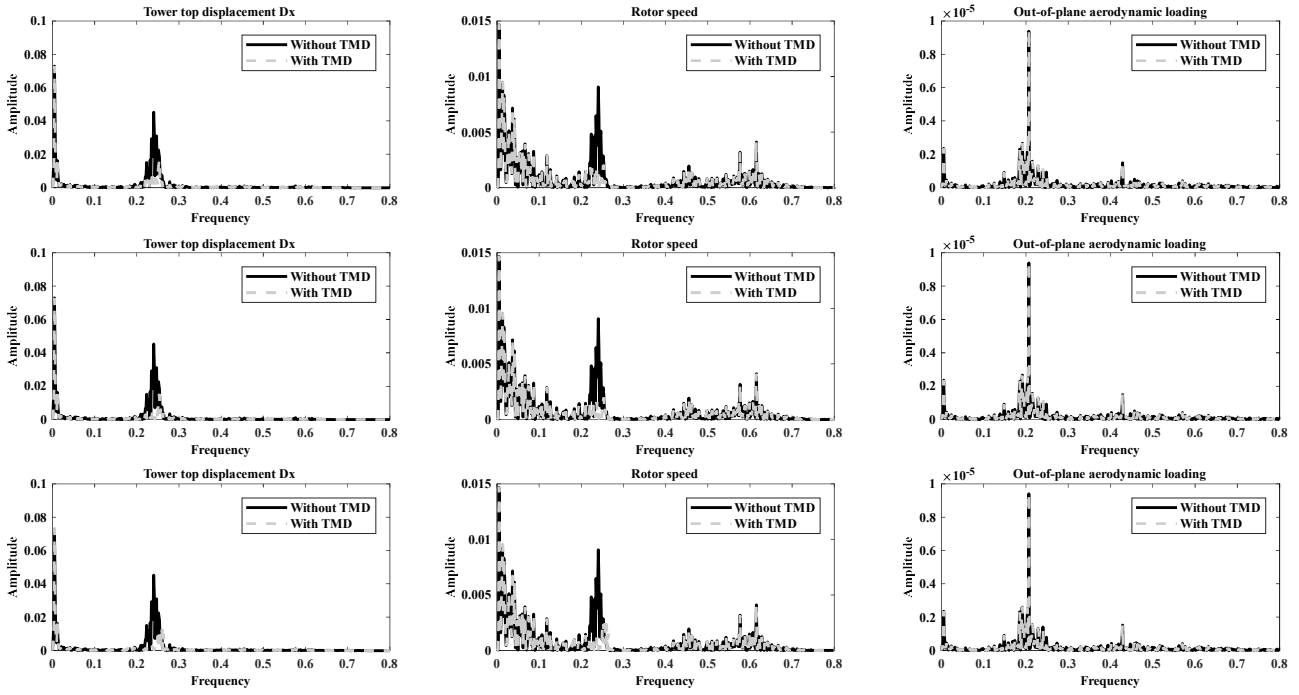

Figure 20. Fourier Transforms of tower top displacement Dx, rotor speed and out-of-plane aerodynamic loading without and with TMD for V=15 m/s, tuning frequency=0.2 Hz; mass ratios: 1% (1st row), 2% (2nd row), 5% (3rd row).

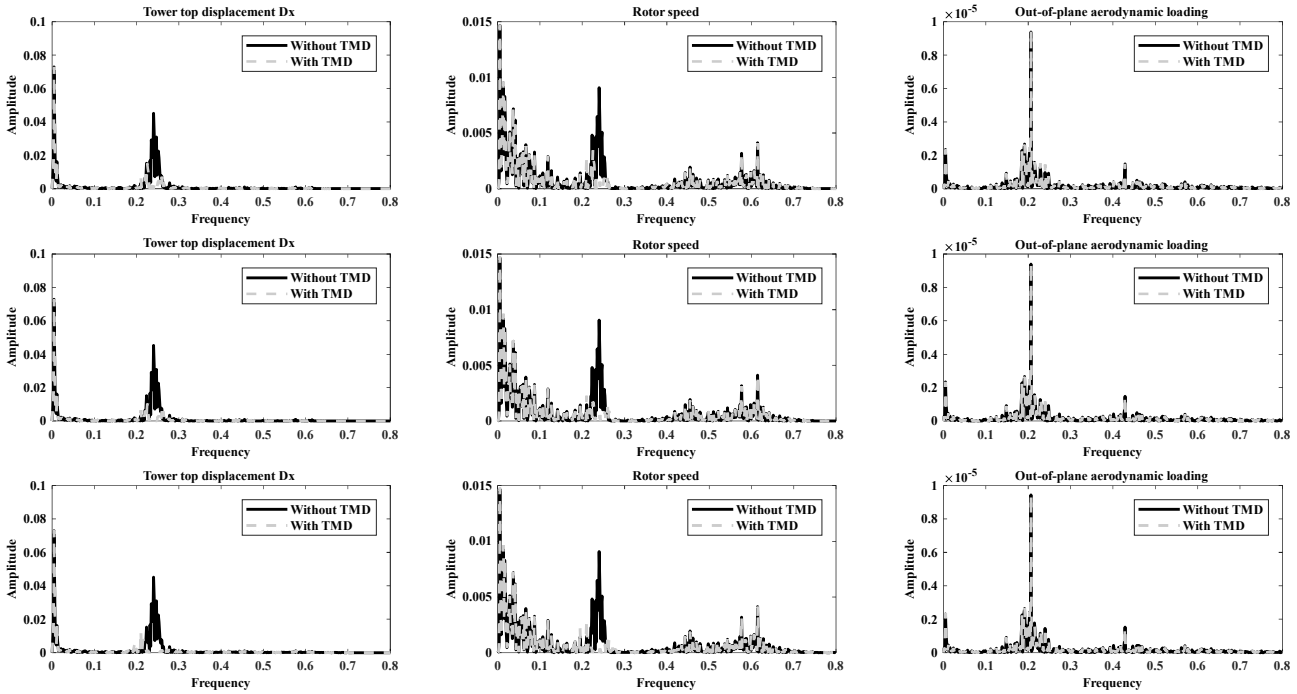

Figure 21. Fourier Transforms of tower top displacement Dx, rotor speed and out-of-plane aerodynamic loading without and with TMD for V=15 m/s, tuning frequency=0.24 Hz; mass ratios: 1% (1st row), 2% (2nd row), 5% (3rd row).

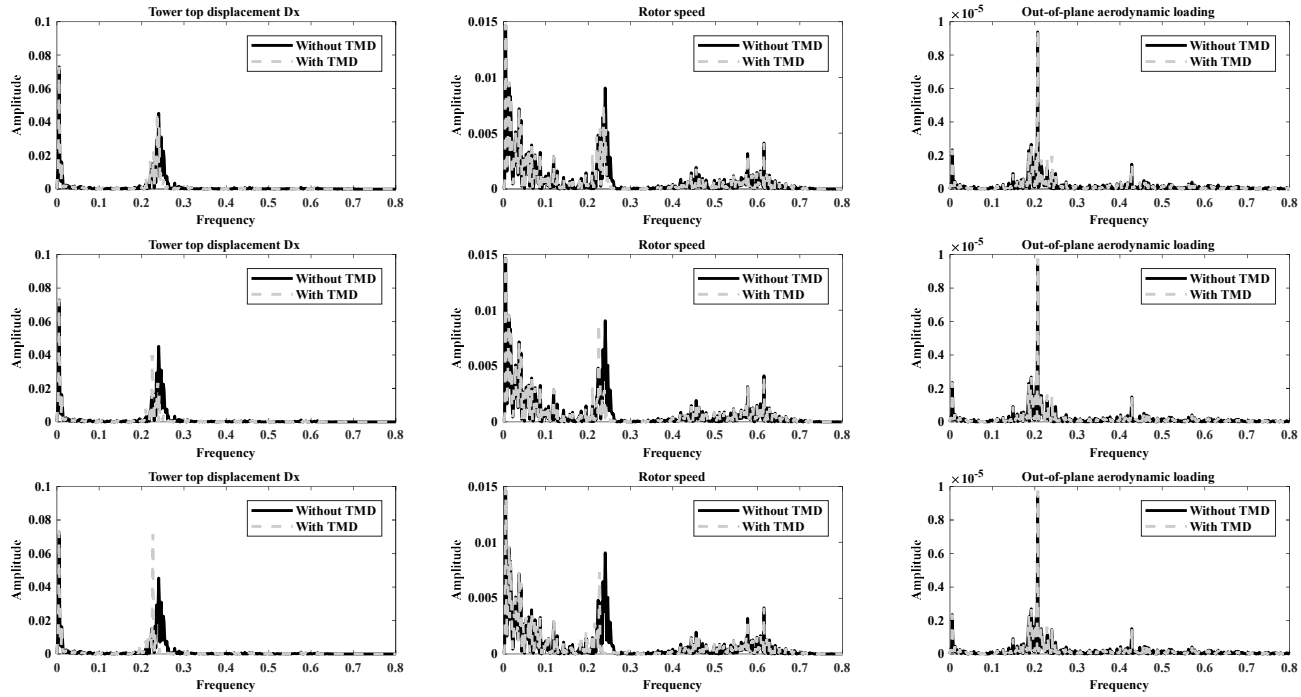

Figure 22. Fourier Transforms of tower top displacement Dx, rotor speed and out-of-plane aerodynamic loading without and with TMD for V=15 m/s, tuning frequency=0.28 Hz; mass ratios: 1% (1st row), 2% (2nd row), 5% (3rd row).

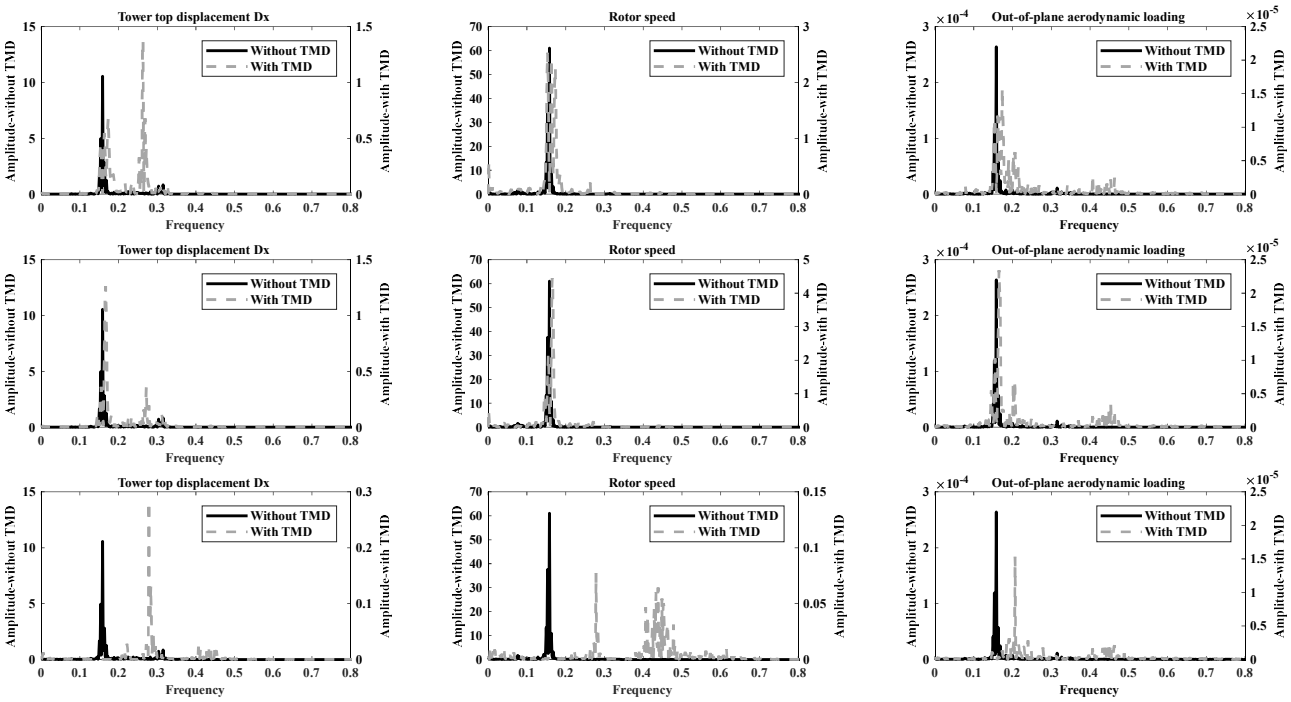

Figure 23. Fourier Transforms of tower top displacement Dx, rotor speed and out-of-plane aerodynamic loading without and with TMD for V=20 m/s, tuning frequency=0.24 Hz; mass ratios: 1% (1st row), 2% (2nd row), 5% (3rd row).

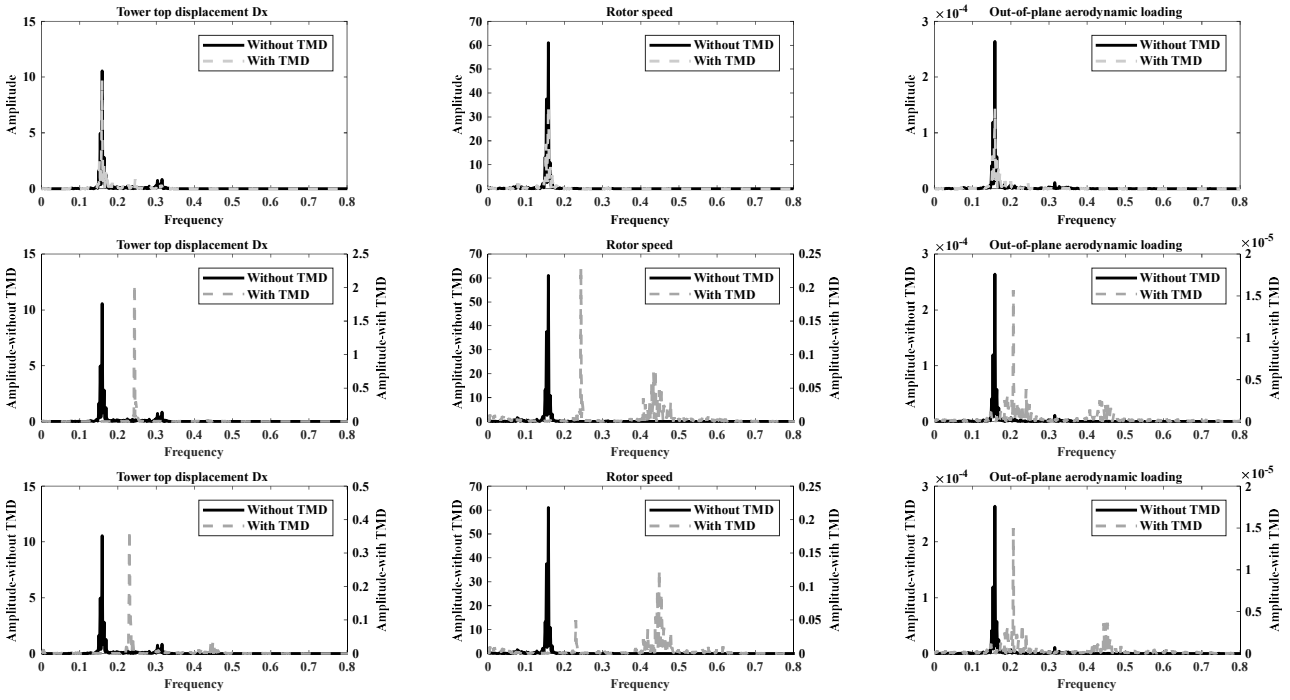

Figure 24. Fourier Transforms of tower top displacement Dx, rotor speed and out-of-plane aerodynamic loading without and with TMD for V=20 m/s, tuning frequency=0.28 Hz; mass ratios: 1% (1st row), 2% (2nd row), 5% (3rd row).

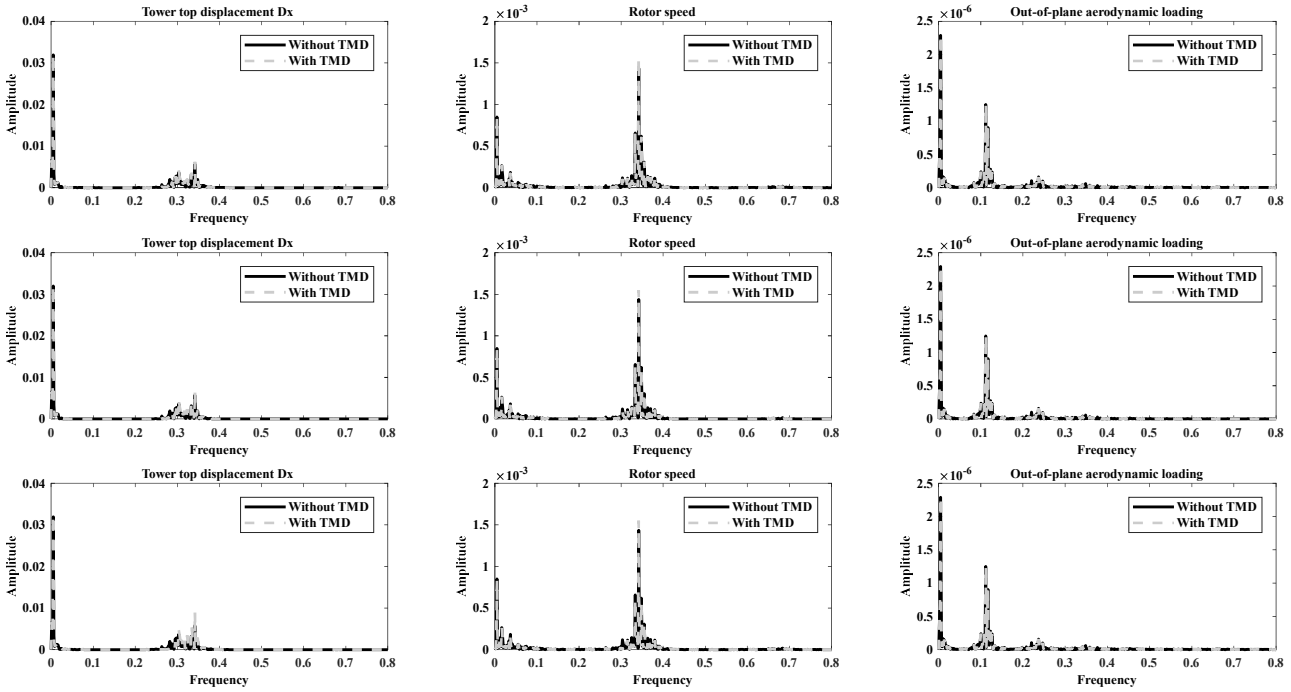

Figure 25. Fourier Transforms of tower displacement Dx, rotor speed and out-of-plane aerodynamic loading without and with TMD for V=5 m/s, tuning Frequency=0.24 Hz; mass ratios: 1% (1st row), 2% (2nd row), 5% (3rd row).

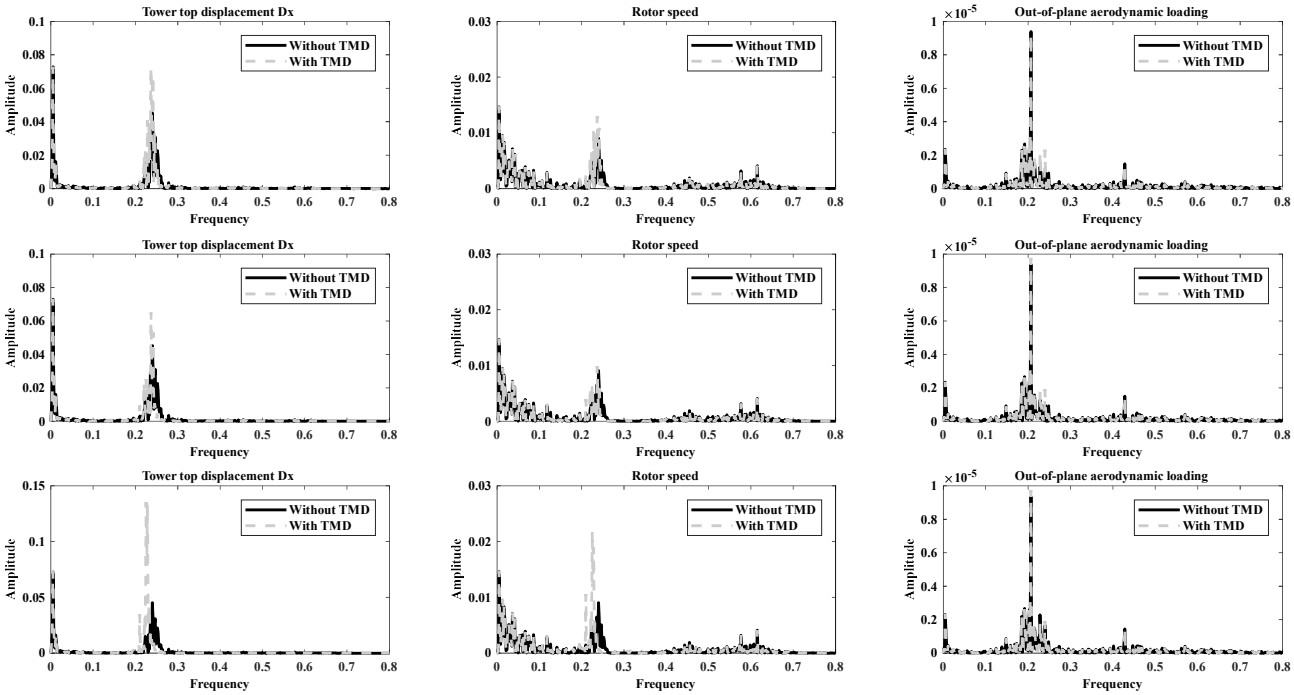

Figure 26. Fourier Transforms of tower top displacement Dx, rotor speed and out-of-plane aerodynamic loading without and with TMD for V=15 m/s, tuning frequency=0.35 Hz; mass ratios: 1% (1st row), 2% (2nd row), 5% (3rd row).

Next, the results in Table 2 for the parked rotor state are examined. For all the considered wind velocities, i.e. V=30 m/s, V=35 m/s and V=40 m/s, the TMD provides a reduction in the standard deviation of the tower top displacement Dx. In general, maxima reductions are attained at the tuning frequency 0.28 Hz, which coincides with the natural frequency of the first fore-aft mode. This result seems to confirm that, without rotor aerodynamics, the system behavior is close to that of a linear system. Also, TMD performances at the tuning frequency 0.28 Hz generally improve as the mass ratio increases from 1% to 5%. A different effect of mass ratio on TMD behavior is found for V=30 m/s, as indeed for mass ratio = 5% the best tuning frequency switches from 0.28 Hz to 0.24 Hz. The FTs pertinent to this case are reported in Figure 27. A general comment on TMD effectiveness in the rotor parked state is that quite good performances of the TMD are obtained also as the tuning frequency moves away from 0.28 Hz, meaning that TMD design is robust also to detuning.

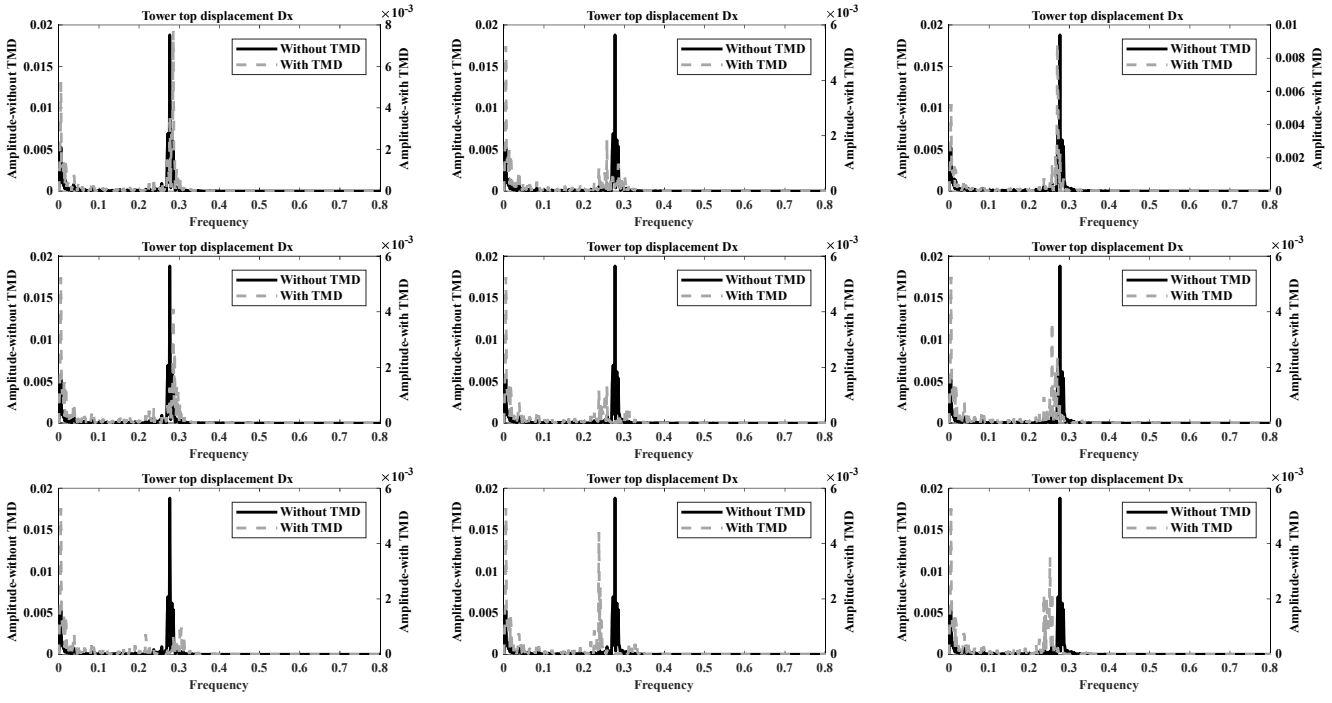

Figure 27. Fourier Transforms of tower top displacement Dx without and with TMD for V=30 m/s; tuning frequencies =0.24 Hz (left), 0.28 Hz (center), 0.31 Hz (right); mass ratios: 1% (1st row); 2% (2nd row); 5% (3rd row).

6.2. Side-to-side response with TMD

Further observations on the system dynamics with TMD concern the standard deviation of the Dy tower top displacement, which are reported in Table 3 for all tuning frequencies, mass ratios, wind velocities considered in Table 2.

Standard Deviation Changes (%)-D_y									
Mass ratio	Frequency (Hz)	Wind speed (m/s)							
		V=5	V=11.4	V=15	V=20	V=24	V=30	V=35	V=40
1%	**0.16**	-0.5007	-0.1358	-4.1186	-3.6439	-11.3576	-0.5383	-1.4497	-1.0387
	0.2	-1.7997	-0.4753	-7.8355	-9.7139	-1.2203	-2.8393	-3.6479	-2.8664
	0.24	-5.3586	-1.1372	-14.1154	-34.5607	-24.1955	-5.9755	-7.3963	-6.1000
	0.28	-8.9986	-2.1726	-19.9235	-23.9767	-30.9623	-7.5100	-13.2160	-9.7534
	0.31	-8.9175	-0.6450	-10.4750	-10.0759	-25.0732	-4.4118	-6.8697	-4.0498
	0.35	-13.0582	+0.4583	-2.2697	+1.9117	-24.2404	-2.2703	-2.6686	-0.7074
2%	**0.16**	-1.2855	-0.2461	-6.9748	-9.6107	-18.0760	-2.2103	-3.3476	-2.6098
	0.2	-2.9635	-0.6620	-11.2528	-8.9486	-17.0825	-4.4411	-6.5031	-4.7824
	0.24	-5.4263	-1.5191	-18.9927	-50.8494	-29.3817	-9.6018	-12.9985	-9.3278
	0.28	-6.0622	-2.2490	-22.2569	-57.3783	-24.3219	-8.4257	-17.0207	-12.4682
	0.31	-6.4547	-0.5347	-14.7402	-3.7773	-30.5111	-4.5303	-9.2976	-6.1622
	0.35	-19.1340	+0.8911	-7.0832	-4.4267	-17.7382	-2.1372	-3.4083	-1.6460
5%	**0.16**	-2.0433	-0.4498	-11.7373	-25.5184	-24.1341	-5.1681	-6.7747	-4.2131
	0.2	-1.7050	-1.0524	-18.3934	-4.7061	-24.6609	-10.5322	-12.4244	-8.8935
	0.24	+1.5291	-1.9774	-23.8381	-64.8519	-23.0956	-12.9048	-16.3770	-13.4923
	0.28	+3.5047	-1.4512	-22.3717	-64.8185	-18.5486	-7.2643	-19.3051	-13.4845
	0.31	-4.2084	-0.8062	-12.9040	-25.1993	-33.1006	-2.3127	-14.9207	-9.9759
	0.35	-26.3464	+1.1203	-7.3318	-8.6294	-21.9001	+0.9815	-6.2911	-3.6388

Table 3. Variations in standard deviation tower top displacement Dy after TMD application.

Regarding the operational rotor state in Table 3, results appear consistent with those in Table 2, i.e. the TMD proves ineffective for V = 11.4 m/s while reductions of the standard deviation are obtained for the other operational wind velocities. Again, the tuning frequencies providing maxima reductions vary with wind velocities as well as mass ratios: e.g., for V=15 m/s maximum reduction is attained at 0.28 Hz with

1% and 2% mass ratio, at 0.24 Hz with 5% mass ratios; for V = 24 m/s at 0.28 Hz with 1%, at 0.31 Hz with 2% and 5% mass ratio. Also, maxima reductions generally increase with the mass ratio. Examples of good performances of the TMD are provided in Figures 28-29. As for the fore-aft response, the conclusion is that the TMD is effective when reduces the frequency content in the FT of the in-plane aerodynamic loading and/or rotor speed.

A further comment on the side-to-side response in the operational rotor state concerns the results for 1% and 2% mass ratios, shown in Table 3: when the tuning frequency is 0.28 Hz, i.e. the natural frequency of the first side-to-side support-structure mode, the TMD always provides a reduction in the standard deviation of the tower top displacement Dy (although not always the optimal one). This result holds for all operational wind velocities, except the rated speed 11.4 m/s, and seems consistent with the FTs in Figures 11-15, which show that Dy is dominated by the first support-structure mode in side-to-side direction. Notice that a similar result is not encountered, instead, in the fore-aft response reported in Table 2.

As for the rotor parked state, comments agree with those on the fore-aft response in Table 2. That is, a reduction in the standard deviation of the tower top displacement Dy is obtained for all wind velocities V=30 m/s, V=35 m/s and V=40 m/s, with maxima generally attained at the tuning frequency 0.28 Hz coinciding with the natural frequency of the first side-to-side support-structure mode. TMD performances at the tuning frequency 0.28 Hz generally improve with the mass ratio. However, effects of mass ratio are different for V=30 m/s as in this case, in agreement with results in Table 2, the best tuning frequency switches from 0.28 Hz to 0.24 Hz as the mass ratio increases.

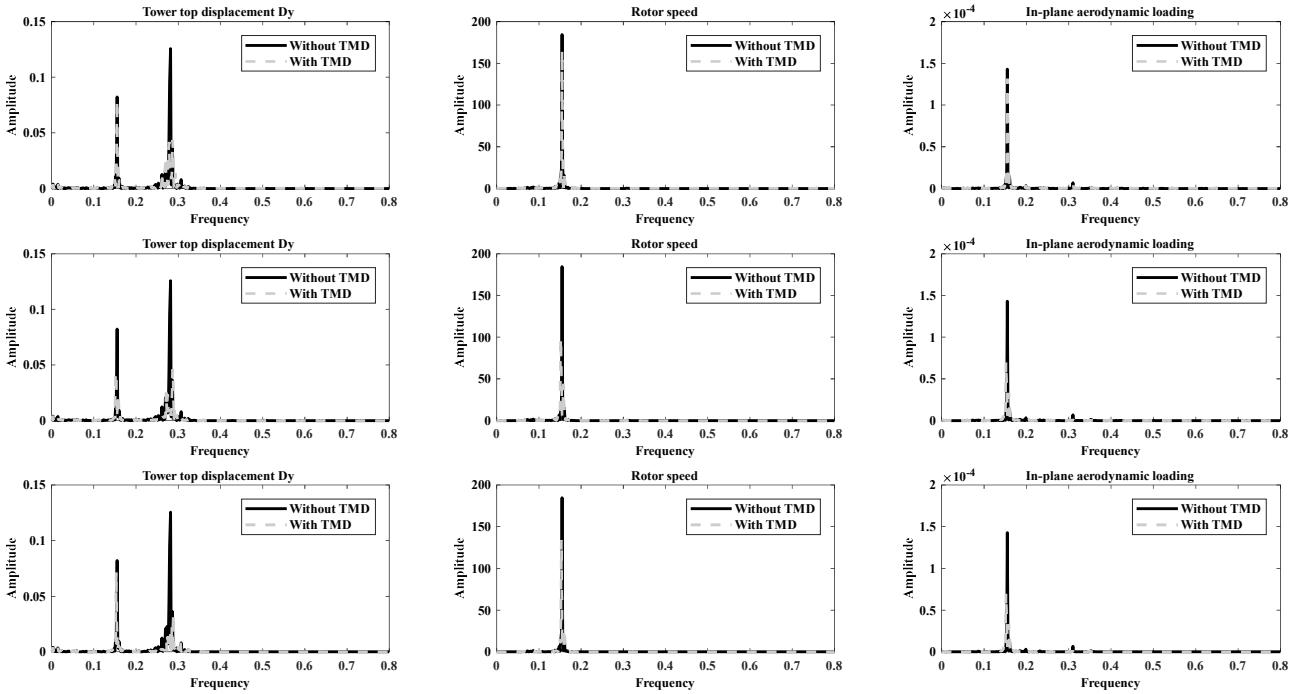

Figure 28. Fourier Transforms of tower top displacement in *y* direction, rotor speed and in-plane aerodynamic loading without and with TMD for V=24 m/s, tuning frequency=0.16 Hz; mass ratios: 1% (1st row), 2% (2nd row), 5% (3rd row).

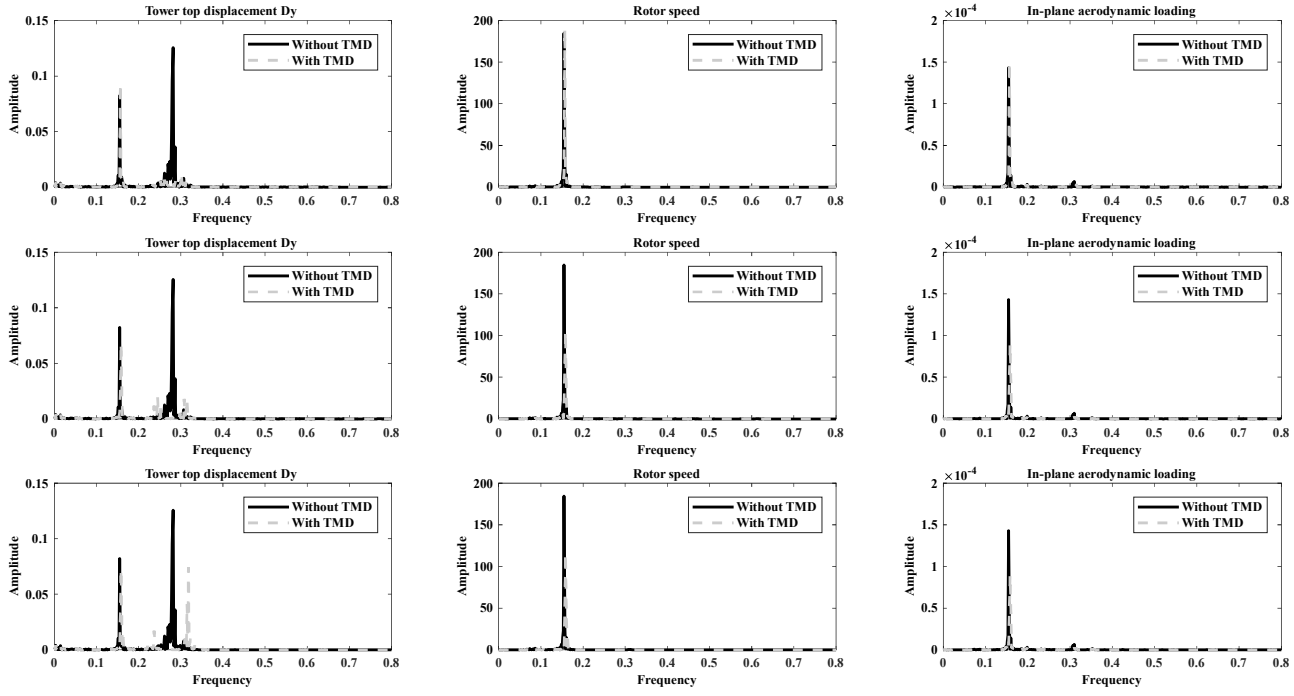

Figure 29. Fourier Transforms of tower top displacement in y direction, rotor speed and in-plane aerodynamic loading without and with TMD for V=24 m/s, tuning frequency=0.28 Hz; mass ratios: 1% (1st row), 2% (2nd row), 5% (3rd row).

6.3. TMD displacements and power production

At this point, in order to gain additional insight into the system response, it is of interest to assess relevant issues such as TMD displacements and power production, for all wind velocities, tuning frequencies and mass ratios considered in Tables 2-3.

Table 4 reports TMD displacements in x direction. Mean values are within few centimeters and maxima values are generally well below 1.0 m; larger maxima values are attained for V=20 m/s and V=24 m/s, with a maximum = 8.4316 m for V=24 m/s, tuning frequency = 0.16 Hz and mass ratio = 2%. This is compatible with the longitudinal dimension of the nacelle of this study (18×6×6 m) and in accordance with typical dimensions in the literature [4]-[5]-[7]. Regarding TMD displacements in y direction, Table 5 shows that the mean is always within few centimeters while the maximum never exceeds 1 m. Also these values are fully compatible with typical dimensions of the nacelle [4]-[5]-[7], including the dimensions selected in this study.

Table 6 shows how mean and standard deviation of the power production, computed over the 600-s simulation, vary with respect to the corresponding values for the system without TMD. In general, variations in Table 6 are very small, meaning that the TMD does not affect the power production of the turbine. It is noticed, however, that for V=20 m/s, tuning frequency range 0.24-0.31 Hz and 5% mass ratio, the TMD has a positive effect on power production, because the mean increases and the standard deviation reduces.

Tuned Mass Damper Displacement X-Direction (m)										
	Mass ratio	Frequency (Hz)	Wind speed (m/s)							
			V=5	V=11.4	V=15	V=20	V=24	V=30	V=35	V=40
Maximum (m)	1%	**0.16**	0.1232	0.4063	0.3738	8.0046	8.2437	0.1658	0.2691	0.3286
		0.2	0.1420	0.4247	0.4895	4.8063	3.6997	0.1713	0.2691	0.3654
		0.24	0.2054	0.2747	0.6670	5.9312	3.4568	0.1997	0.3265	0.4228
		0.28	0.3203	0.2217	0.5791	3.9474	3.5858	0.2151	0.4195	0.5465
		0.31	0.4100	0.1747	0.4615	2.7815	3.1967	0.1600	0.3220	0.3490
		0.35	0.2698	0.1282	0.3636	1.3916	1.6089	0.0955	0.1671	0.2449
	2%	**0.16**	0.1257	0.3939	0.3593	8.1140	8.4316	0.1511	0.2792	0.3368
		0.2	0.1419	0.3901	0.4720	3.5333	3.7855	0.1648	0.2510	0.3384
		0.24	0.1912	0.2622	0.6748	5.2659	3.3575	0.1661	0.2631	0.3794
		0.28	0.2731	0.2138	0.4777	2.4463	3.3494	0.1785	0.2688	0.3958
		0.31	0.3389	0.1606	0.3573	3.3101	2.3585	0.1279	0.2267	0.3284
		0.35	0.2246	0.1174	0.3511	1.4540	1.3416	0.0865	0.1560	0.2384
	5%	**0.16**	0.1310	0.3705	0.3181	7.8437	8.3284	0.1663	0.3050	0.3575
		0.2	0.1530	0.3140	0.4399	4.0638	2.8537	0.1397	0.1918	0.2799
		0.24	0.1961	0.2299	0.4922	1.7686	2.4814	0.1158	0.1729	0.2516
		0.28	0.2405	0.1845	0.4429	1.0804	2.2102	0.1105	0.1561	0.2352
		0.31	0.2248	0.1394	0.3511	1.7993	1.5043	0.0988	0.1288	0.2071
		0.35	0.1403	0.1048	0.2487	1.8828	0.9658	0.0690	0.1069	0.1729
Mean (m)	1%	**0.16**	0.0181	0.0835	0.0625	0.0478	0.0431	0.0072	0.0116	0.0167
		0.2	0.0116	0.0536	0.0401	0.0346	0.0287	0.0046	0.0074	0.0107
		0.24	0.0080	0.0370	0.0273	0.0213	0.0215	0.0034	0.0053	0.0076
		0.28	0.0061	0.0282	0.0209	0.0115	0.0154	0.0026	0.0040	0.0058
		0.31	0.0048	0.0222	0.0164	0.0133	0.0095	0.0019	0.0031	0.0045
		0.35	0.0037	0.0174	0.0130	0.0112	0.0100	0.0015	0.0024	0.0035
	2%	**0.16**	0.0181	0.0836	0.0624	0.0295	0.0626	0.0073	0.0116	0.0167
		0.2	0.0116	0.0536	0.0401	0.0356	0.0264	0.0047	0.0074	0.0107
		0.24	0.0080	0.0371	0.0275	0.0239	0.0187	0.0034	0.0053	0.0076
		0.28	0.0061	0.0282	0.0210	0.0162	0.0132	0.0025	0.0040	0.0058
		0.31	0.0048	0.0222	0.0165	0.0142	0.0119	0.0019	0.0031	0.0045
		0.35	0.0038	0.0174	0.0130	0.0109	0.0087	0.0015	0.0025	0.0035
	5%	**0.16**	0.0181	0.0836	0.0625	0.0492	0.0404	0.0073	0.0116	0.0168
		0.2	0.0116	0.0535	0.0402	0.0329	0.0263	0.0047	0.0075	0.0109
		0.24	0.0080	0.0371	0.0278	0.0215	0.0198	0.0033	0.0052	0.0075
		0.28	0.0061	0.0282	0.0210	0.0164	0.0153	0.0025	0.0040	0.0059
		0.31	0.0048	0.0222	0.0165	0.0120	0.0120	0.0020	0.0031	0.0045
		0.35	0.0038	0.0174	0.0130	0.0095	0.0094	0.0015	0.0024	0.0035

Table 4. TMD displacement in *x* direction.

Tuned Mass Damper Displacement Y-Direction (m)										
	Mass ratio	Frequency (Hz)	Wind speed (m/s)							
			V=5	V=11.4	V=15	V=20	V=24	V=30	V=35	V=40
Maximum (m)	1%	**0.16**	0.0282	0.0406	0.0814	0.5678	0.7660	0.4264	0.6582	0.6110
		0.2	0.0361	0.0448	0.0892	0.3973	0.5671	0.5592	0.7158	0.6703
		0.24	0.0455	0.0404	0.0984	0.7148	0.5736	0.6444	0.9407	0.8320
		0.28	0.0580	0.0442	0.1087	0.5041	0.5660	0.6684	1.0319	1.1693
		0.31	0.0880	0.0409	0.0830	0.4557	0.5376	0.5737	0.8456	1.0211
		0.35	0.0823	0.0279	0.0615	0.2654	0.2992	0.3603	0.4242	0.5916
	2%	**0.16**	0.0280	0.0399	0.0780	0.6306	0.7696	0.3993	0.6563	0.5810
		0.2	0.0340	0.0446	0.0803	0.4261	0.4206	0.5583	0.6736	0.6669
		0.24	0.0409	0.0384	0.0895	0.4158	0.7000	0.5946	0.8897	0.7244
		0.28	0.0534	0.0372	0.0844	0.2317	0.5376	0.5794	0.8489	0.9198
		0.31	0.0873	0.0317	0.0614	0.4395	0.4645	0.4626	0.7113	0.8428
		0.35	0.0650	0.0261	0.0481	0.2357	0.2696	0.3535	0.3732	0.4731
	5%	**0.16**	0.0265	0.0414	0.0713	0.5314	0.7354	0.4102	0.6368	0.6260
		0.2	0.0285	0.0405	0.0752	0.3859	0.3404	0.5022	0.5992	0.6388
		0.24	0.0402	0.0322	0.0548	0.1445	0.4002	0.4594	0.6446	0.5340
		0.28	0.057	0.0286	0.0463	0.1556	0.4939	0.4756	0.6016	0.5734
		0.31	0.0702	0.0248	0.0602	0.2275	0.2775	0.4093	0.4188	0.4671
		0.35	0.0414	0.0215	0.0388	0.1786	0.2815	0.3327	0.3142	0.3911
Mean (m)	1%	**0.16**	0.0024	0.0139	0.0157	0.0146	0.0161	0.0032	0.0045	0.0050
		0.2	0.0015	0.0089	0.0101	0.0100	0.0096	0.0018	0.0029	0.0029
		0.24	0.0010	0.0062	0.0070	0.0071	0.0064	0.0013	0.0026	0.0027
		0.28	0.0008	0.0047	0.0053	0.0049	0.0052	0.0010	0.0016	0.0020
		0.31	0.0007	0.0037	0.0042	0.0038	0.0039	0.0007	0.0008	0.0016
		0.35	0.0005	0.0029	0.0033	0.0031	0.0031	0.0007	0.0008	0.0012
	2%	**0.16**	0.0024	0.0139	0.0157	0.0137	0.0165	0.0032	0.0046	0.0050
		0.2	0.0015	0.0089	0.0101	0.0099	0.0092	0.0018	0.0029	0.0029
		0.24	0.0010	0.0062	0.0070	0.0071	0.0072	0.0013	0.0024	0.0025
		0.28	0.0008	0.0047	0.0053	0.0055	0.0052	0.0011	0.0017	0.0021
		0.31	0.0007	0.0037	0.0042	0.0042	0.0039	0.0007	0.0009	0.0016
		0.35	0.0005	0.0029	0.0033	0.0033	0.0032	0.0007	0.0008	0.0012
	5%	**0.16**	0.0024	0.0139	0.0157	0.0145	0.0149	0.0032	0.0047	0.0052
		0.2	0.0015	0.0089	0.0101	0.0099	0.0097	0.0017	0.0029	0.0030
		0.24	0.0011	0.0062	0.0071	0.0072	0.0068	0.0014	0.0022	0.0024
		0.28	0.0008	0.0047	0.0054	0.0055	0.0051	0.0009	0.0016	0.0021
		0.31	0.0007	0.0037	0.0042	0.0042	0.0041	0.0009	0.0012	0.0016
		0.35	0.0005	0.0029	0.0033	0.0031	0.0032	0.0007	0.0009	0.0012

Table 5. TMD displacement in *y* direction.

Power Production							
	Mass ratio	Frequency (Hz)	Wind speed (m/s)				
			V=5	V=11.4	V=15	V=20	V=24
Mean (m)	1%	**0.16**	-0.0016	+0.0050	+0.0182	+0.2228	+0.1765
		0.2	-0.0050	+0.0041	+0.0275	-0.0808	+0.1692
		0.24	-0.0130	+0.0047	+0.0300	+9.8502	+0.1596
		0.28	-0.0308	+0.0034	+0.0167	+1.0213	+0.4124
		0.31	-0.0460	+0.0036	-0.0077	+1.2041	+0.4258
		0.35	-0.0376	+0.0047	-0.0169	+0.2969	+0.0256
	2%	**0.16**	-0.0071	+0.0054	+0.0261	+0.1114	+0.2930
		0.2	-0.0125	+0.0029	+0.0298	-0.2479	+0.1201
		0.24	-0.0271	+0.0038	+0.0316	+9.8918	+0.0954
		0.28	-0.0577	+0.0025	+0.0277	+12.6067	+0.4740
		0.31	-0.0805	+0.0041	+0.0100	+1.8241	+0.1567
		0.35	-0.0565	+0.0052	-0.0059	+0.3034	+0.2655
	5%	**0.16**	-0.0226	+0.0045	+0.0302	+0.8179	+0.8133
		0.2	-0.0387	+0.0041	+0.0279	-0.1273	+0.1264
		0.24	-0.0734	+0.0014	+0.0334	+12.6912	+0.4474
		0.28	-0.1147	+0.0011	+0.0298	+12.6440	+0.5007
		0.31	-0.1475	+0.0007	-0.0051	+7.3643	+0.3113
		0.35	-0.0679	+0.0038	+0.0080	+1.2019	+0.0080
Standard Deviation (m)	1%	**0.16**	-0.0017	-0.0097	-1.9423	-1.1456	-0.2626
		0.2	-0.0046	-0.0124	-2.9799	-0.1968	-0.1609
		0.24	-0.0086	-0.0160	-3.1171	-44.3589	-0.6528
		0.28	-0.0154	-0.0126	-1.3059	-2.8815	-0.5911
		0.31	-0.0359	-0.0135	+1.3875	-2.3765	+1.0672
		0.35	-0.0331	-0.0162	+2.6039	0.6590	+0.5678
	2%	**0.16**	-0.0097	-0.0126	-2.7385	-1.4806	-0.8504
		0.2	-0.0108	-0.0090	-3.4687	-0.0381	-0.7404
		0.24	-0.0125	-0.0140	-3.3697	-44.0499	-0.2977
		0.28	-0.0160	-0.0112	-2.4120	-70.0155	+0.0008
		0.31	-0.0770	-0.0151	-0.6278	-2.7777	+2.1794
		0.35	-0.0302	-0.0149	+1.1574	+0.5908	+1.9552
	5%	**0.16**	-0.0262	-0.0199	-3.5052	-2.7469	-2.4379
		0.2	-0.0211	-0.0064	-3.3888	-0.7269	-1.0180
		0.24	-0.0251	-0.0122	-3.5138	-70.5695	+0.0275
		0.28	-0.0696	-0.0058	-2.8800	-70.3942	+0.9738
		0.31	-0.1449	-0.0053	+1.4344	-25.6214	+4.0612
		0.35	-0.0240	-0.0128	-0.3907	-1.8613	+3.3242

Table 6. Power production after TMD application.

Finally, Table 7 summarizes the results reported in Tables 2-3-4-5-6 for the TMD tuning frequency that provides the best reduction in the standard deviation of the tower top displacement Dx. This is of particular interest considering that tower top displacements in the *x* direction are larger than those in *y* direction (see previous comments on Figures 11-18 vs. Figures 3-10). Specifically, variations in standard deviation of tower top displacements Dx and Dy, TMD displacements in *x* and *y* direction, as well as variations in mean and standard deviation of power production, are reported in Table 7 for all wind velocities and TMD mass ratios. The general comments are that, for every wind velocity except for the rated speed V=11.4 m/s, the TMD provides appreciable reductions in the standard deviation of Dx as well as Dy, with acceptable displacements of the TMD and no significant changes in power production, except for the case V=20 m/s where its mean increases and its standard deviation reduces. It is also apparent that the optimal tuning frequency varies with wind velocity as well as mass ratio. Best results, however, are generally obtained for 5% mass ratio. This is an important conclusion in view of practical design as indeed, once a 5% mass ratio is chosen, an adjustable stiffness could allow the TMD to be actively tuned to the optimal frequency as wind velocity varies. Examples of adjustable-stiffness TMD already exists, see among others ref. [34]-[35]-[36].

Optimal TMD Parameters								
Wind speed	**Mass ratio**	**Optimal Tuning Frequency (Hz)**	**Dx Displ. Standard Deviation (%)**	**Dy Displ. Standard Deviation (%)**	**TMD Maximum Displacement X direction (m)**	**TMD Maximum Displacement Y direction (m)**	**Power Production Standard Deviation (%)**	**Power Production Mean (%)**
5 m/s	**1%**	0.35	-8.9846	-13.0582	0.2698	0.0823	-0.0376	-0.0331
	2%	0.35	-14.1071	-19.1340	0.2246	0.0650	-0.0565	-0.0302
	5%	0.35	-20.8415	-26.3464	0.1403	0.0414	-0.0679	-0.0240
11.4 m/s	**1%**	0.2	-0.1901	-0.4753	0.4247	0.0448	+0.0041	-0.0124
	2%	0.16	-0.2732	-0.2461	0.3939	0.0399	+0.0054	-0.0126
	5%	0.16	-0.5019	-0.4498	0.3705	0.0414	+0.0045	-0.0199
15 m/s	**1%**	0.24	-23.2551	-14.1154	0.6670	0.0984	+0.0300	-3.1171
	2%	0.24	-25.1738	-18.9927	0.6748	0.0895	+0.0316	-3.3697
	5%	0.24	-25.7926	-23.8381	0.4922	0.0548	+0.0334	-3.5138
20 m/s	**1%**	0.24	-36.3316	-34.5607	5.9312	0.7148	+9.8502	-44.3589
	2%	0.28	-67.8895	-57.3783	2.4463	0.2317	+12.6067	-70.0155
	5%	0.28	-79.8730	-64.8185	1.0804	0.1556	+12.6440	-70.3942
24 m/s	**1%**	0.31	-5.9295	-25.0732	3.1967	0.5376	+0.4258	+1.0672
	2%	0.31	-7.3441	-30.5111	2.3585	0.4645	+0.1567	+2.1794
	5%	0.31	-6.6894	-33.1006	1.5043	0.2775	+0.3113	+4.0612
30 m/s	**1%**	0.28	-30.6995	-7.5100	0.2151	0.6684	-	-
	2%	0.28	-31.9352	-8.4257	0.1785	0.5794	-	-
	5%	0.24	-32.8322	-12.9048	0.1158	0.4594	-	-
35 m/s	**1%**	0.28	-24.6625	-13.2160	0.4195	1.0319	-	-
	2%	0.28	-27.6274	-17.0207	0.2688	0.8489	-	-
	5%	0.28	-30.4613	-19.3051	0.1561	0.6016	-	-
40 m/s	**1%**	0.28	-29.6998	-9.7534	0.5465	1.1693	-	-
	2%	0.28	-33.5252	-12.4682	0.3958	0.9198	-	-
	5%	0.28	-37.4314	-13.4845	0.2352	0.5734	-	-

Table 7. TMD optimal parameters.

7. CONCLUDING REMARKS

This paper has studied vibration mitigation in offshore HAWTs, focusing on the baseline 5-MW NREL HAWT with an omnidirectional TMD in the nacelle, mounted on a monopile in shallow waters. Building on a preliminary investigation of the system dynamics without TMD, a wide range of potential tuning

frequencies and mass ratios have been selected for the TMD, under various wind velocities in operational and rotor parked states. The main conclusions are as follows.

In the rotor parked state, the TMD is effective at every considered tuning frequency, with best performances generally obtained at tuning frequency = natural frequency of first fore-aft and side-to-side support-structure modes. This is evidence that system behavior is close to linearity when no rotor aerodynamics is involved.

In the operational rotor state, the TMD is ineffective at the rated wind speed V=11.4 m/s because, in this case, tower top oscillations are small. At the other operational wind velocities, the TMD is effective but at selected tuning frequencies, which vary with wind velocity. This is attributable to inherent non-linearity of rotor dynamics. In general, numerical simulations show that the TMD is effective when reduces the frequency content of aerodynamic loading and/or rotor speed.

For both parked and operational rotor states, best TMD performances are generally obtained for 5% mass ratio. Maxima TMD displacements are compatible with typical dimensions of the nacelle and no significant changes occur in the power production, with the only exception of V=20 m/s where, for the optimal TMD tuning frequency, mean increases and standard deviation reduces.

The relevant conclusion of this study is that optimal performances of the TMD can be obtained as long as the tuning frequency is changed depending on the wind velocity. Therefore, a conventional design based on a fixed tuning frequency = natural frequency of first support-structure modes does not seem appropriate. On the contrary, once the mass ratio is fixed, a TMD with adjustable stiffness [34]-[35]-[36] could be appropriately tuned to the best frequency depending on the wind velocity.

8. APPENDIX

This Appendix contains the FTs of out-of-plane and in-plane aerodynamic loading at some stations along the blade. The purpose is to show that, as stated in the main text, the frequency content in the FTs calculated at various stations is similar. Here, the case V=11.4 m/s and V=15 m/s are considered but analogous results are obtained for the other wind velocities, omitted for brevity.

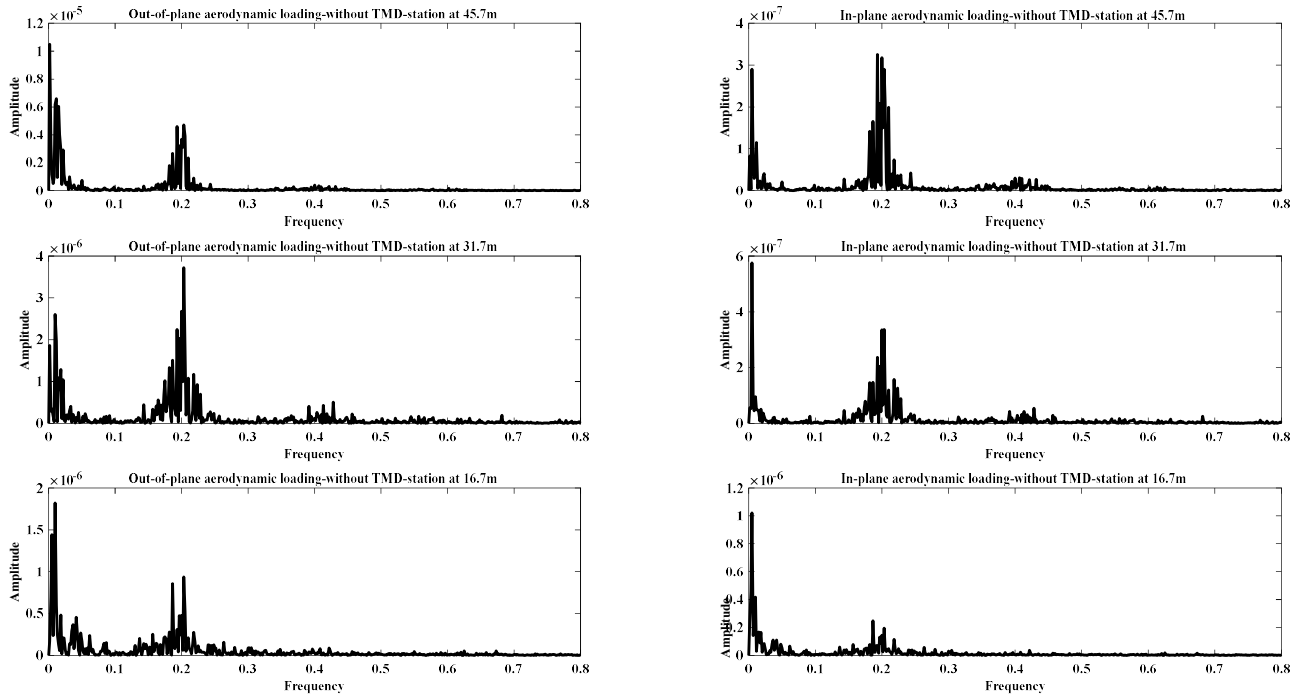

Figure 30. Fourier Transforms of aerodynamic loadings at different blade stations, for V=11.4 m/s.

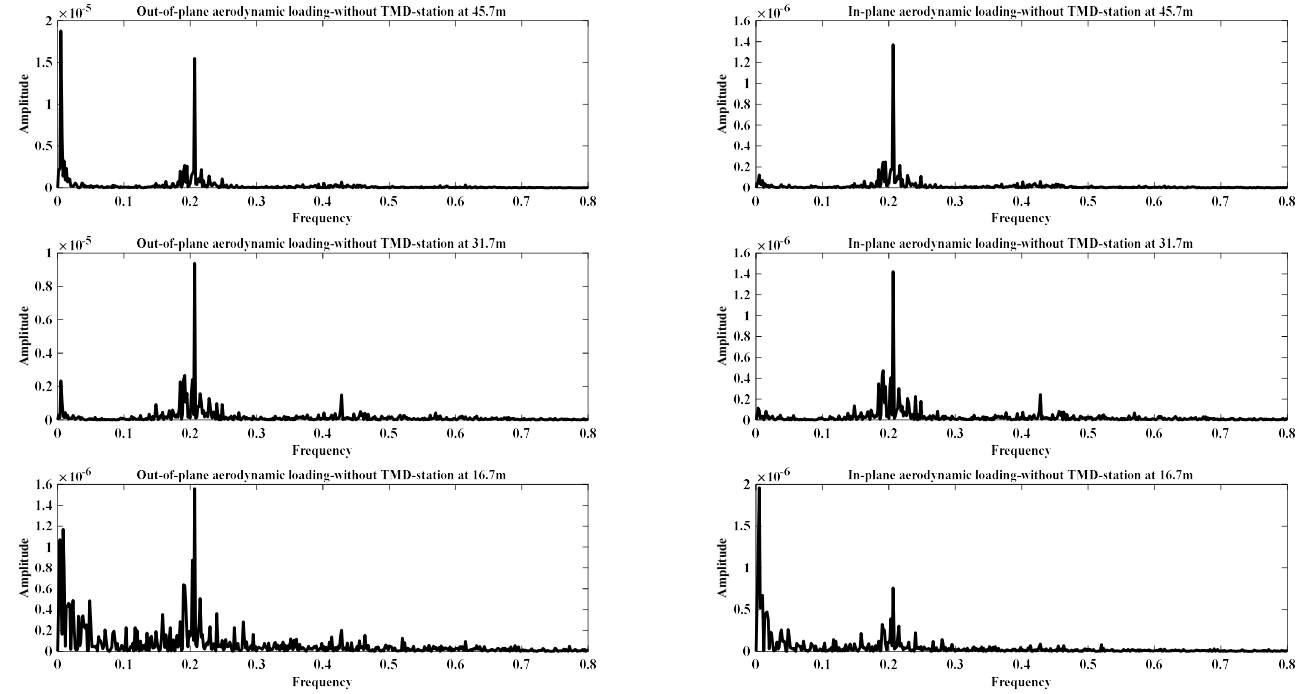

Figure 31. Fourier Transforms of aerodynamic loadings at different blade stations, for V=15 m/s.

9. REFERENCES

[1] Failla G, Arena F. New perspectives in offshore wind energy. Phil. Trans. R. Soc. A 2015; 373(2035): 20140228.

[2] Rendon EA, Manuel L. Long-term loads for a 41onopole-supported offshore wind turbine. Wind Energy 2014; 17(2): 209-223.

[3] Soong T, Spencer B. Supplemental energy dissipation: state-of-the-art and state-of-the-practice. Eng. Struct. 2002; 24: 243-59.

[4] Lackner MA, Rotea MA. Passive structural control of offshore wind turbines. Wind Energy 2011; 14: 373-88.

[5] Jonkman J, Buhl ML. Fast user's guide. Technical Report NREL/EL-500-38230, National Renewable Energy laboratory, Golden, CO, 2006.

[6] Stewart G, Lackner M. Offshore wind turbine load reduction employing optimal passive tuned mass damping systems. IEEE Transactions on Control Systems Technology 2013; 21(4): 1090-104.

[7] Stewart GM, Lackner MA. The impact of passive tuned mass dampers and wind-wave misalignment on offshore wind turbine loads. Eng. Struct. 2014; 73: 54-61.

[8] Zuo H, Bi K, Hao H. Using multiple tuned mass dampers to control offshore wind turbine vibrations under multiple hazards. Eng. Struct. 2017, 141: 303-315.

[9] Dassault Systèmes Simulia Corp. Abaqus 6.14 Scripting User's Guide. Dassault Systèmes Simulia Corp., Providence, RI, 2014.

[10] Si Y, Karimi HR, Gao H. Modelling and optimization of a passive structural control design for a spar-type floating wind turbine. Eng. Struct. 2014; 69: 168-182.

[11] Altay O, Meinerzhagen ML, Taddei F, Butenweg C, Klinkel S. Seismic protection of wind turbines using tuned mass dampers. In: Proceedings of the 2nd European Conference on Earthquake Engineering and Seismology, Istanbul, August 25-29, 2014.

[12] Murtagh PJ, Ghosh A, Basu B, Broderick BM. Passive control of wind turbine vibrations including blade/tower interaction and rotationally sampled turbulence. Wind Energy 2008; 11: 305-17.

[13] Murtagh PJ, Basu B, Broderick BM. Along-wind response of a wind turbine tower with blade coupling subjected to rotationally sampled wind loading. Eng. Struct. 2005; 27: 1209-19.

[14] Enevoldsen I, Mørk KJ. Effects of a vibration mass damper in a wind turbine tower. Mechanics of Structures and Machines: An International Journal 1996; 24(2): 155-87.

[15] Colwell S, Basu B. Tuned liquid column dampers in offshore wind turbines for structural control. Eng. Struct. 2009; 31: 358-68.

[16] Mensah AF, Dueñas-Osorio L. Improved reliability of wind turbine towers with tuned liquid column dampers (TLCDs). Struct. Saf. 2014; 47: 78-86.

[17] Lackner MA, Rotea MA. Structural control of floating wind turbines. Mechatronics 2011; 21: 704-19.

[18] Stewart GM, Lackner MA The effect of actuator dynamics on active structural control of offshore wind turbines. Eng. Struct. 2011; 33: 1807-16.

[19] Fitzgerald B, Basu B, Nielsen SRK. Active tuned mass dampers for control of in-plane vibrations of wind turbine blades. Struct. Control Health Monit. 2013; 20:1377-96.

[20] Arrigan J, Pakrashi V, Basu B, Nagarajaiah S. Control of flapwise vibrations in wind turbine blades using semi-active tuned mass dampers. Struct. Control Health Monit. 2011; 18: 840-51.

[21] Zhang Z, Basu B, Nielsen SRK. Tuned liquid column dampers for mitigation of edgewise vibrations in rotating wind turbine blades. Struct. Control Health Monit. 2015; 22: 500-17.

[22] Bossanyi EA. Bladed for windows user manual. Garrad Hassan and Partners, Bristol, 2000.

[23] Jonkman J, Musial W. Offshore code comparison collaboration (OC3) for IEA – Task 23 offshore wind technology and deployment. Report No. NREL/TP-5000-48191, National Renewable Energy Laboratory (NREL), Golden, CO, 2010.

[24] Jonkman J, Butterfield S, Musial W, Scott G. Definition of a 5-MW reference wind turbine for offshore system development. Report No. NREL/TP-500-38060, National Renewable Energy Laboratory (NREL), Golden, CO, 2009.

[25] Santangelo F, Failla G, Arena F, Ruzzo C. On time-domain uncoupled analyses for offshore wind turbines under seismic loads. Bull. Earthquake Eng. 2018; 16(2): 1007-40.

[26] Alati N, Failla G, Arena F. Seismic analysis of offshore wind turbines on bottom-fixed support structures. Phil. Trans. R. Soc. A 2015; 373: 20140086.

[27] International Electrotechnical Commission (IEC). Wind turbines-part 1: design requirements. IEC 61400-1, 3rd ed., Geneva, 2005.

[28] Manwell JF, McGowan JG, Rogers AL. Wind energy explained: theory, design and application. Wiley, Chichester, 2010.

[29] International Electrotechnical Commission (IEC). Wind turbines-part 3: design requirements for offshore wind turbines. IEC 61400-3, 1st ed., Geneva, 2009.

[30] Det Norske Veritas (DNV). Design of offshore wind turbine structures. DNV-OS-J101, Copenhagen, 2013.

[31] Ernst B, Seume JR. Investigation of site-specific wind field parameters and their effect on loads of offshore wind turbines. Energies 2012; 5: 3835-55.

[32] Resor BR. Definition of a 5 MW/61.5 m wind turbine blade reference model. Report no. SAND2013-2569, Wind Energy Technology Department Sandia National Laboratories, Albuquerque, NM, 2013.

[33] Leu TS, Yo JM, Tsai YT, Miau JJ, Wang TC. Assessment of IEC 61400-1 normal turbulence model for wind conditions in Taiwan west coast areas. In: Proceedings of 5th international symposium on physics fluids (ISPF5), Int. J. Modern Phys. 2014; 34: 1460382.

[34] Spencer BF, Nagarajaiah S. State-of-the-art of structural control. J. Struct. Eng. 2003; 129(7): 845-56.

[35] Nagarajaiah S, Varadarajan N. Short time Fourier transform algorithm for wind response control of buildings with variable stiffness TMD. Eng. Struct. 2005; 27: 431-41.

[36] Nagarajaiah S, Sonmez E. Structures with semiactive variable stiffness single/multiple tuned mass dampers. J. Struct. Eng. 2007; 133(1): 67-77.

FIGURE CAPTIONS

Figure 1. Test structure.

Figure 2. First and second support-structure modes in *x* direction.

Figure 3. Fourier Transforms of response variables in *x* direction, for V=5 m/s.

Figure 4. Fourier Transforms of response variables in *x* direction, for V=11.4 m/s.

Figure 5. Fourier Transforms of response variables in *x* direction, for V=15 m/s.

Figure 6. Fourier Transforms of response variables in *x* direction, for V=20 m/s.

Figure 7. Fourier Transforms of response variables in *x* direction, for V=24 m/s.

Figure 8. Fourier Transforms of response variables in *x* direction, for V=30 m/s.

Figure 9. Fourier Transforms of response variables in *x* direction, for V=35 m/s.

Figure 10. Fourier Transforms of response variables in *x* direction, for V=40 m/s.

Figure 11. Fourier Transforms of response variables in *y* direction, for V=5 m/s.

Figure 12. Fourier Transforms of response variables in *y* direction, for V=11.4 m/s.

Figure 13. Fourier Transforms of response variables in *y* direction, for V=15 m/s.

Figure 14. Fourier Transforms of response variables in y direction for V=20 m/s.

Figure 15. Fourier Transforms of response variables in y direction for V=24 m/s.

Figure 16. Fourier Transforms of response variables in *y* direction, for V=30 m/s.

Figure 17. Fourier Transforms of response variables in *y* direction, for V=35 m/s.

Figure 18. Fourier Transforms of response variables in *y* direction, for V=40 m/s.

Figure 19. Fourier Transforms of tower top displacement Dx, rotor speed and out-of-plane aerodynamic loading without and with TMD for V=5 m/s, tuning frequency=0.35 Hz; mass ratios: 1% (1st row), 2% (2nd row), 5% (3rd row).

Figure 20. Fourier Transforms of tower top displacement Dx, rotor speed and out-of-plane aerodynamic loading without and with TMD for V=15 m/s, tuning frequency=0.2 Hz; mass ratios: 1% (1st row), 2% (2nd row), 5% (3rd row).

Figure 21. Fourier Transforms of tower top displacement Dx, rotor speed and out-of-plane aerodynamic loading without and with TMD for V=15 m/s, tuning frequency=0.24 Hz; mass ratios: 1% (1st row), 2% (2nd row), 5% (3rd row).

Figure 22. Fourier Transforms of tower top displacement Dx, rotor speed and out-of-plane aerodynamic loading without and with TMD for V=15 m/s, tuning frequency=0.28 Hz; mass ratios: 1% (1st row), 2% (2nd row), 5% (3rd row).

Figure 23. Fourier Transforms of tower top displacement Dx, rotor speed and out-of-plane aerodynamic loading without and with TMD for V=20 m/s, tuning frequency=0.24 Hz; mass ratios: 1% (1st row), 2% (2nd row), 5% (3rd row).

Figure 24. Fourier Transforms of tower top displacement Dx, rotor speed and out-of-plane aerodynamic loading without and with TMD for V=20 m/s, tuning frequency=0.28 Hz; mass ratios: 1% (1st row), 2% (2nd row), 5% (3rd row).

Figure 25. Fourier Transforms of tower displacement Dx, rotor speed and out-of-plane aerodynamic loading without and with TMD for V=5 m/s, tuning Frequency=0.24 Hz; mass ratios: 1% (1st row), 2% (2nd row), 5% (3rd row).

Figure 26. Fourier Transforms of tower top displacement Dx, rotor speed and out-of-plane aerodynamic loading without and with TMD for V=15 m/s, tuning frequency=0.35 Hz; mass ratios: 1% (1st row), 2% (2nd row), 5% (3rd row).

Figure 27. Fourier Transforms of tower top displacement Dx without and with TMD for V=30 m/s; tuning frequencies =0.24 Hz (left), 0.28 Hz (center), 0.31 Hz (right); mass ratios: 1% (1st row); 2% (2nd row); 5% (3rd row).

Figure 28. Fourier Transforms of tower top displacement in *y* direction, rotor speed and in-plane aerodynamic loading without and with TMD for V=24 m/s, tuning frequency=0.16 Hz; mass ratios: 1% (1st row), 2% (2nd row), 5% (3rd row).

Figure 29. Fourier Transforms of tower top displacement in y direction, rotor speed and in-plane aerodynamic loading without and with TMD for V=24 m/s, tuning frequency=0.28 Hz; mass ratios: 1% (1st row), 2% (2nd row), 5% (3rd row).

Figure A.1. Fourier Transforms of aerodynamic loadings at different blade stations, for V=11.4 m/s.

Figure A.2. Fourier Transforms of aerodynamic loadings at different blade stations, for V=15 m/s.

TABLE CAPTIONS

Table 1. Modal frequencies.

Table 2. Variations in standard deviation of tower top displacement Dx after TMD application.

Table 3. Variations in standard deviation tower top displacement Dy after TMD application.

Table 4. TMD displacement in x direction.

Table 5. TMD displacement in y direction.

Table 6. Power production after TMD application.

Table 7. TMD optimal parameters.

Declarations of interest: none